Design of a Biomechanically Synergistic Exotendon Suit

by

Carmen Marten-Ellis Graves

S.B. Mechanical Engineering
Massachusetts Institute of Technology, 2011

SUBMITTED TO THE DEPARTMENT OF MECHANICAL ENGINEERING IN PARTIAL FULFILLMENT OF THE REQUIREMENTS FOR THE DEGREE OF

MASTER OF SCIENCE IN MECHANICAL ENGINEERING
AT THE
MASSACHUSETTS INSTITUTE OF TECHNOLOGY

SEPTEMBER 2013

Signature of Author:_____
Department of Mechanical Engineering
August 9, 2013

Certified by:_____
Sangbae Kim
Assistant Professor of Mechanical Engineering
Thesis Supervisor

Accepted by:_____
David E. Hardt
Ralph E. and Eloise F. Cross Professor of Mechanical Engineering
Chairman, Department Committee on Graduate Students

Design of a Biomechanically Synergistic Exotendon Suit

by

Carmen Marten-Ellis Graves

Submitted to the Department of Mechanical Engineering
on August 9, 2013 in partial fulfillment of the
Requirements for the Degree of Master of Science in
Mechanical Engineering

Abstract

The focus of this thesis is on the design, development, and evaluation of a lightweight, exotendon suit for load carriage. The suit is intended to be worn underneath the wearer's own clothes for use in a military setting, while reducing the energy expenditure of the wearer. A simple exotendon suit architecture was designed and implemented, consisting of two knee braces, a length of polypropylene tendon, a belt, two electro-magnet clutches, and a control box. The electro-magnet clutches are mounted at the waist and tendons are used to apply the actuator's force to the wearer's ankles. This is advantageous, as many current exoskeletons mount actuators at the ankles, requiring a greater amount of additional energy expenditure.

Testing was performed at the Wyss Institute for Biologically Inspired Engineering Motion Capture Laboratory. Metabolic power was tested using a COSMED K4b2 system and surface electromyogram (sEMG) data was collected using a Delsys Trigno system. Five male subjects participated in six trials, walking on a treadmill at 1.25 m/s, carrying a 20 kg load in a standard military rucksack. The six trials consisted of three conditions: street clothes, exosuit worn but unpowered (passive), and exosuit word and powered (active). Results of the tests were inconclusive. There was no significant evidence that powering the exosuit has a positive or negative effect on the wearer's energy usage.

Thesis Supervisor: Sangbae Kim
Title: Assistant Professor of Mechanical Engineering

Acknowledgements

I would like to thank Professor Sangbae Kim for all of his support throughout this project. He has provided me with the resources to allow this project to become an invaluable experience. Thanks to Dr. Hae Won Park and Dr. Dong Jin Hyun for their assistance with the suit's controller and thanks to Professor Conor Walsh, Dr. Patrick Aubin and Dr. Stefano de Rossi for their help with experimental testing at the Wyss Institute for Biologically Inspired Engineering Motion Capture Laboratory.

Special thanks to my mother, my father, my brother, and Delmy for never giving up on me. And thanks to Joshua Ramos for standing by me and supporting me when I thought I would not finish. You all mean so much to me. Love you all.

Table of Contents

List of Figures

List of Tables

1 Introduction

The applications for lower body exoskeletons in the world today are endless. Exoskeletons have the capacity to help users ranging from patients with lower-extremity impairments and elderly patients with movement restrictions, to able-bodied adults, such as military soldiers carrying heavy rucksacks. Research on powered human exoskeletons has been growing in the past several years and current exoskeletons can now help with load carriage[1,2] and augment joints for injured or elderly users.[3,4] For the most part, the existing exoskeletons require a significant amount of power to apply large torques to joints and are heavy and rigid to support large loads.[5]

For many exoskeleton applications, the primary goal is to reduce energy expenditure of the user. However, only recently have researchers begun to study the metabolic effects of exoskeletons. Starting with Norris[6] in 2007, and later with Sawicki[7] and Lenzi[8], researchers have been designing and building powered exoskeletons for the lower body in hopes of reducing the metabolic energy usage of the user. These groups have managed to demonstrate a lowered metabolic cost of walking with the powered exoskeleton when compared to wearing the exoskeleton unpowered, but not compared to walking without the exoskeleton at all. These systems add weight to the users' extremities, significantly increasing the metabolic energy that needs to be overcome by the exoskeleton.[9] As of today, Sawicki's system is the only known exosytem to reduce metabolic energy usage to below that of walking without the exoskeleton, yet only for specific conditions of constrained step frequency, length, and speed.[10]

The goal of the research in this thesis is the development of a light, soft exotendon suit for lower body assistance for able-bodied adults carrying load, particularly in a military setting. This exotendon suit should reduce the metabolic cost to the wearer, while requiring a lower amount of

power. The strategy employed in this project involves the placement of actuators at the waist as opposed to the ankle, to minimize the weight at the ankle. The actuation is transmitted to the ankle via tendons that traverse the legs, from where the name "exotendon suit" is derived. This approach contrasts greatly those of the systems mentioned earlier with bulky exoskeletons at the ankle. Without the additional mass at the ankles, less additional metabolic energy needs to be overcome to reduce metabolic energy to that to walking without the exotendon suit.

This project is part of a larger Defense Advanced Research Projects Agency (DARPA) Warrior Web Program, focusing on the development of a low-power undersuit to increase endurance and carriage capacity, and reduce injury.

This thesis focuses on the design, development, and evaluation of the exotendon suit for load carriage. Specifically, Chapter 2 describes architecture of the suit, as well as the design and fabrication of the various components that compose the exosuit. Chapter 3 outlines the experimental design, data analysis and results. Metabolic power and EMG data were used to evaluate the suite. Finally Chapter 4 summarizes the conclusions from the thesis and describes possibilities for future work.

2 Exotendon Suit Design and Fabrication

2.1 Suit Architecture

The exotendon suit was designed to be flexible and lightweight, as to not impede the movement of the wearer, the eventual goal being to be worn underneath the wearer's own clothes. Very few rigid components were involved. As the suit is intended for military use, it is designed to be work with combat boots and a rucksack. In addition to the boots and rucksack, the wearer dons clutch actuators, mounted to a belt, and flexible knee wraps, as shown in Figure 2.1. Polypropylene webbing is used as a tendon, spanning the wearer's legs from the clutches to the boots, routed through the knee wraps.

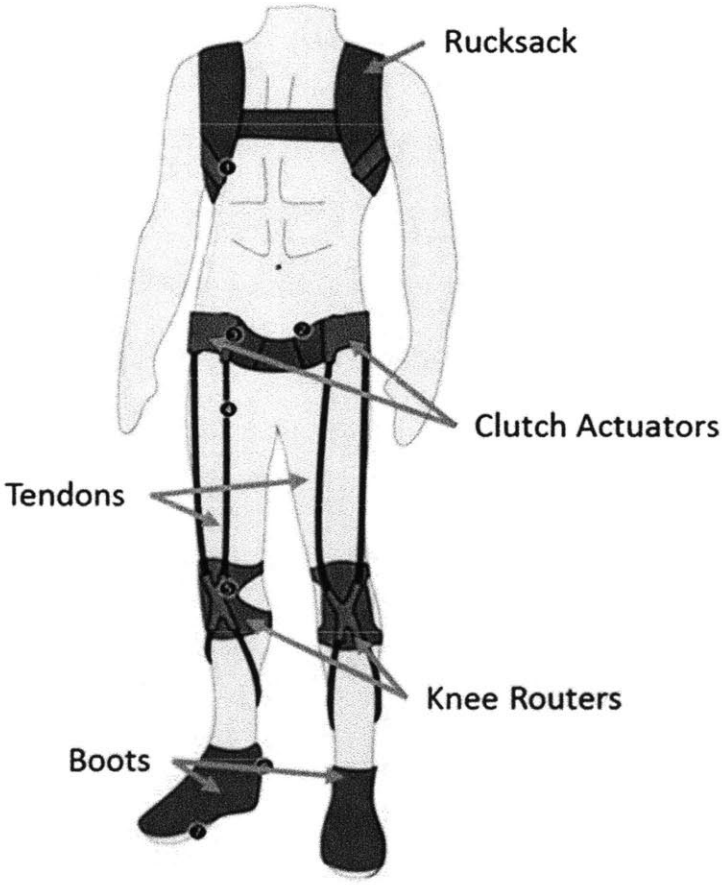

Figure 2.1 Concept drawing of poly-articular exotendon suit.

Using sensors placed within the boots, a microcontroller mounted within the rucksack selectively activates the clutches as the wearer walks to create tension on the tendon, and apply torques to the knee and ankle joint. The wiring and control is further explained in Chapter 2.7.

2.2 Tendon Routing and Knee Joint

The torque applied to the knee by the tension in the tendons varies depending on the tendon routing. The distance from the center of the knee joint that the tendon passes is the radius, and as the radial distance from the center of the knee joint increases, a greater torque is applied to the knee. Two configurations were tested, the full radius of the knee (Figure 2.2a) and a radius of zero (Figure 2.2b).

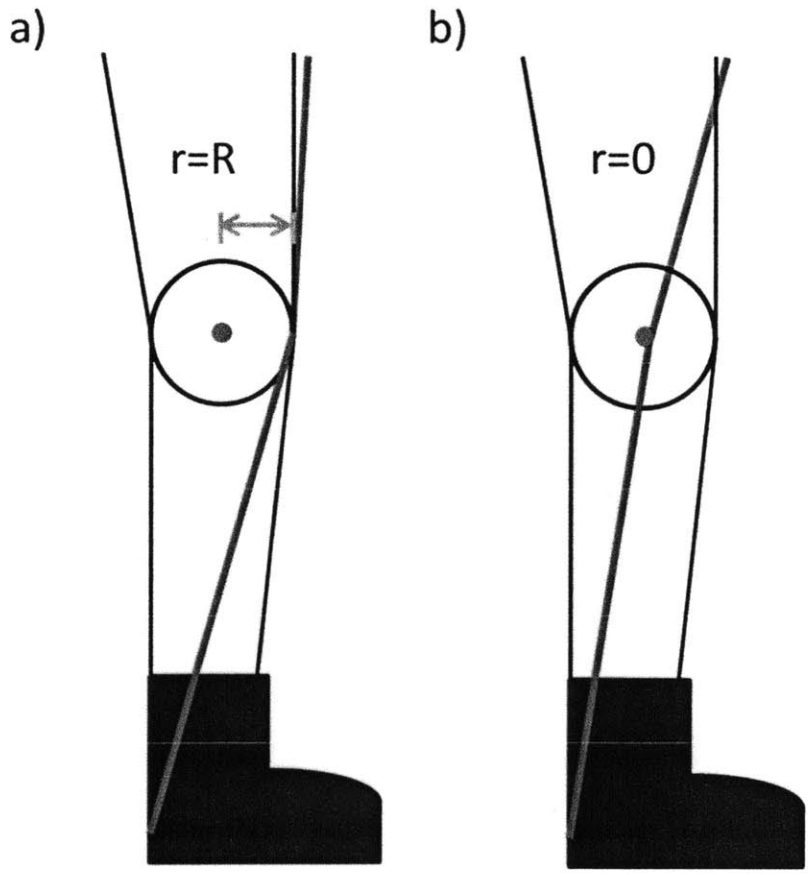

Figure 2.2 Knee routing configurations tested, full knee radius (a), and no radius (b).

Users determined that a torque applied at the full radius of the knee, as in Figure 2.2a was uncomfortable and felt unnatural. A radius of zero was used during the experiments. This zero radius was achieved by sewing sleeves for the tendon on a flexible neoprene knee wrap, as shown in Figure 2.3. The sleeves are sufficiently wide enough to allow the tendon to slide freely along the length of the leg, but do not shift much radially, keeping the tendons at a radius of zero.

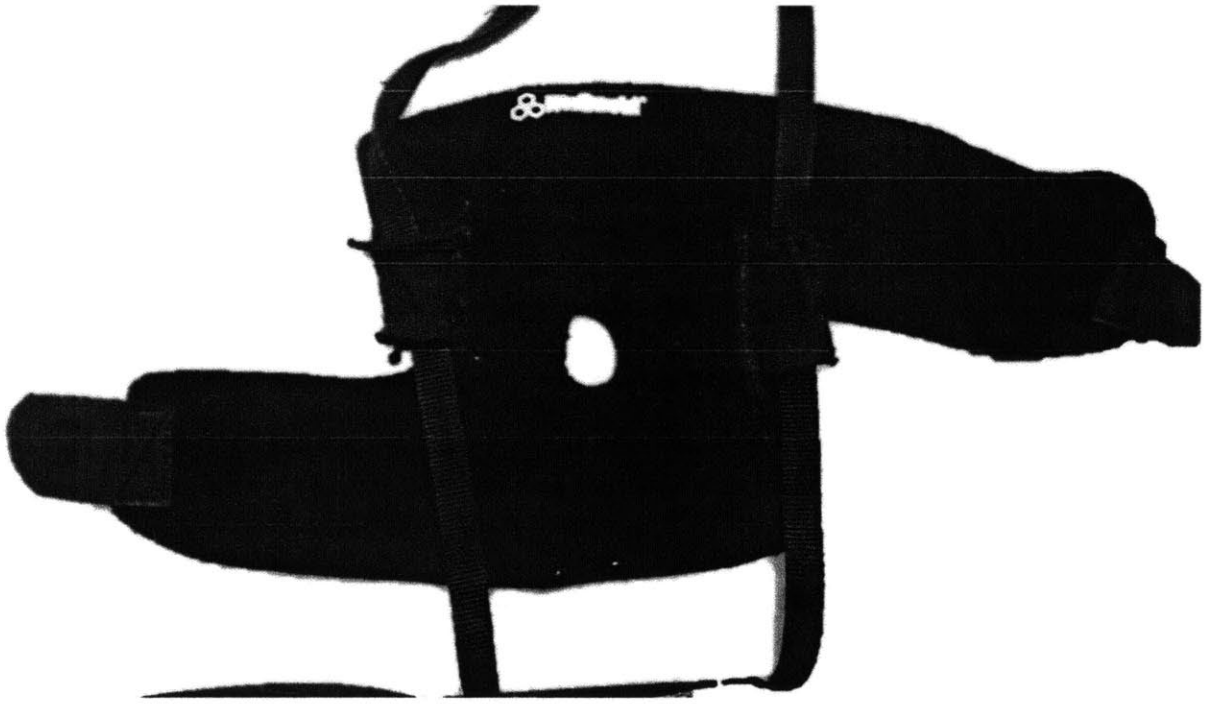

Figure 2.3 Sleeves were sown into a neoprene knee wrap to allow the tendons to slide.

The knee wrap is adjustable to allow for wearers of different sizes. Plastic fittings along the tendons allowed for the length of the tendons to be adjusted for the height of the wearer. The tendons interface with the clutches through the use of buckles, so the suit can be easily donned and doffed.

2.3 Clutch Design

The function of the clutch in the exotendon suit is to selectively apply tension to the tendons traversing the user's legs. While the clutch is not activated, the tendon needs to be free to extend under tension, and otherwise retract and when activated, the clutch needs to brake and lock the tendon. A clock-spring design, similar to that of a tape measure, was implemented in order to allow for the tendon to retract. Electro-permanent magnets and electro-magnets were both considered as actuation methods for the clutch.

2.3.1 Electro-Permanent Magnet

An electro-permanent magnet (EPM) is made up of a magnet with a high coercivity and a magnet core with a low coercivity, encased in a coil and a steel shell as shown in Figure 2.4. In the case proposed, Neodynium-Iron-Boron (NIB) and Aluminum-Nickel-Cobalt (Alnico) were to be used as magnets of high and low coercivity, respectively. The NIB and Alnico magnets are aligned in parallel and a coil is wound around them. When a pulse of current is applied to the coils, the magnetic field created is great enough to switch the magnetization direction of the Alnico magnet, but not of the NIB magnet due to its higher coercivity.

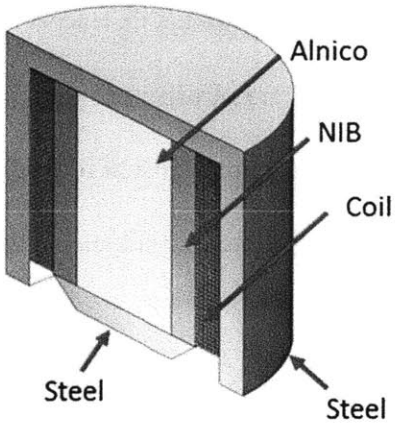

Figure 2.4 A cross section of an EPM. A copper coil is wound around an Alnico and NIB magnet core. Steel comprises the shell.

Figure 2.5 illustrates the two states of the EPM. The EPM is in the on state when the two magnets and their fluxes are aligned within the EPM. The magnetic flux then travels through an adjacent ferromagnetic surface and the surface is attracted to the magnet. The EPM is in the off state when the two magnets and their fluxes are oppositely aligned. In this case, the magnetic flux circulates with the EPM and not through an adjacent ferromagnetic surface.[11]

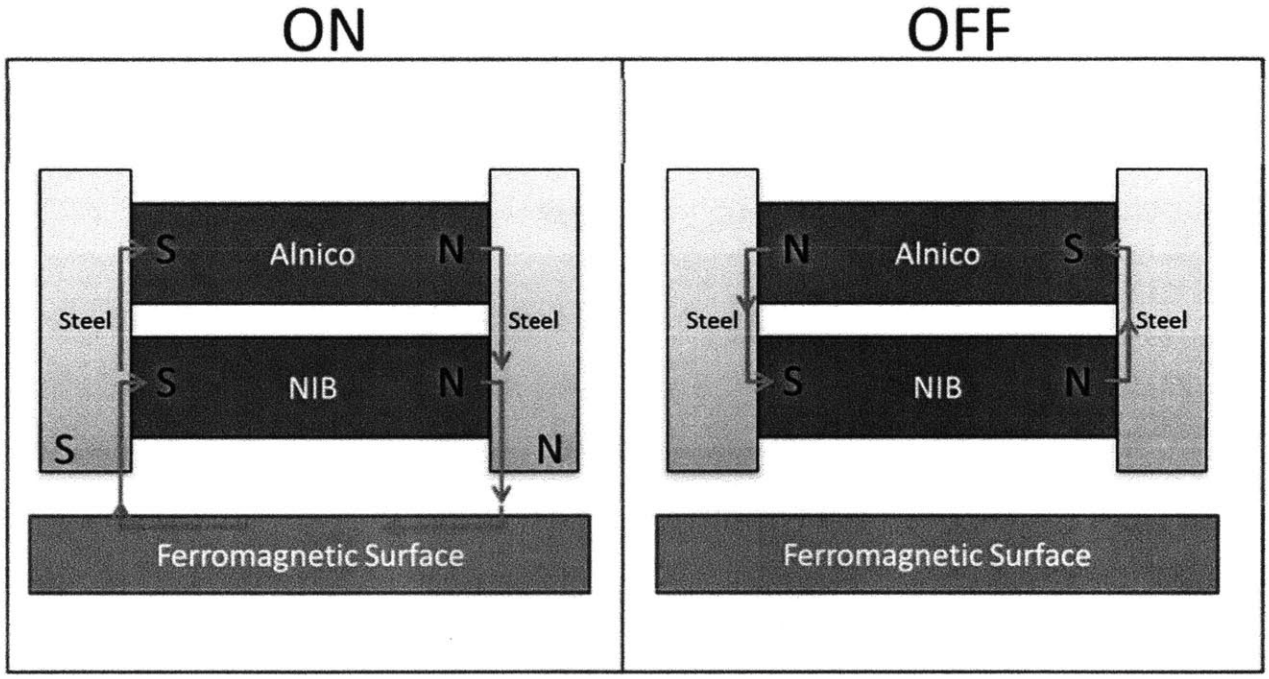

Figure 2.5 The on and off states of an EPM. A pulse of current through a coil can reverse the polarization of the Alnico magnet, changing the state of the EPM.

While the EPM is in either state, power is not consumed. Power is only consumed during the transition period between states when a pulse of current is used to switch the polarity of the Alnico magnet. For this reason, EPMs have the potential for being a very low powered solution for many applications. However, the frequency at which the EPMs would need to switch state for application in human walking is too high for efficient use. Applying a pulse of current

through the coil great enough to change the polarity of the Alnico magnet involves the charging and discharging of a large capacitor. Designing a circuit to charge and discharge a large capacitor at the frequency required for human walking was out of the scope of this thesis. For this reason, an electro-magnet clutch was prototyped.

2.3.2 Electro-Magnet Clutch

In an electro-magnet, a sustained current through a coil magnetizes an iron core, attracting a ferromagnetic surface. Unlike an EPM, an electro-magnet consumes power while in the on state. The first clutch prototypes were designed and fabricated using the off-the-shelf rotary electro-magnet clutch shown in Figure 2.6.

Figure 2.6 The OTS rotary electro-magnet clutch used in the first prototyped clutches. Specifications are included in the Appendix.[12]

These OTS electro-magnet clutches have a holding torque of 9 Nm and use about 8 W of power. Power-On clutches were selected to ensure safety for the user. In the case of a broken connection, the clutches release and should not impede the subject.

2.4 Clock-Spring

The clock-spring was designed to support the weight of the tendon, estimated to be about 1 kg, as to be able to keep the tendon taut while the clutch is not activated. The torque, T, delivered by a clock-spring can be calculated with the equation:

$$\text{[illegible]} \qquad \text{Equation 2.1}$$

where E is the Young's modulus of the spring, b is the width of the material, t is the material thickness, [illegible]s the desired angular rotation in revolutions, and L is the length of material, illustrated in Figure 2.7. Using 0.35 mm thick and 12.7 mm wide spring steel, and a full rotation, the length of material required to provide a torque to support 1 kg at a 20 mm radius was about 200 mm. A cross-section of the clutch with the fabricated clock-spring is shown in section 2.5 in Figure 2.9.

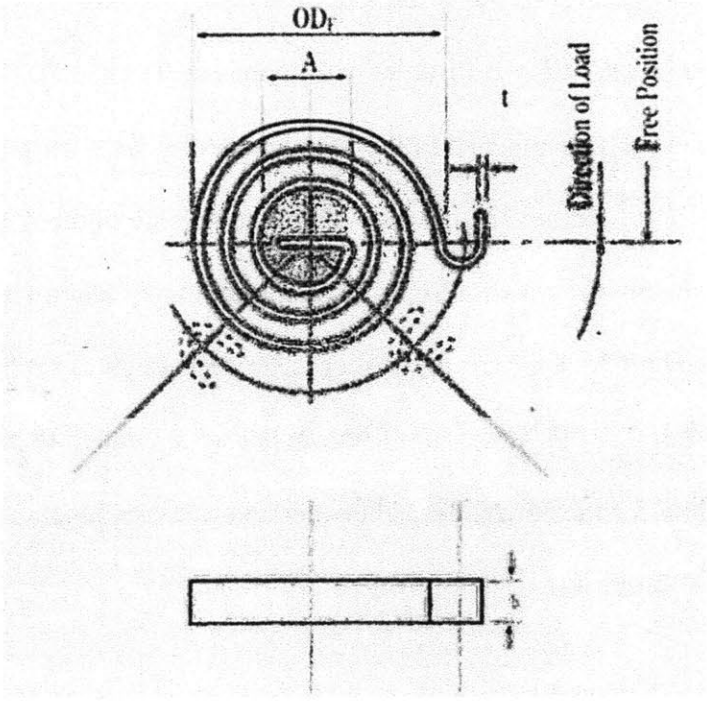

Figure 2.7 Labeled diagram of a clock-spring, illustrating the width, b, and the thickness, t.[13]

2.5 Full Clutch Design

The OTS electro-magnet clutch used consists of two components, a stationary component housing the coil, and a mating rotational part shown in Figure 2.8 in red and blue respectively. In order for the clutch to work as intended, the inner radius of the clock-spring needs to be rigidly attached to the stationary component of the OTS electro-magnet clutch, while the outer radius of the clock-spring needs to be rigidly attached to the mating rotational part. This way, as the mating part rotates, the clock-spring works to restore it to an original position.

This was accomplished by rigidly attaching the stationary component of the OTS electro-magnet clutch and an aluminum shaft (yellow in Figure 2.8) to a base plate to ensure that the shaft and clutch are stationary relative to each other. The mating clutch component is a mounted on the shaft via a sleeve bearing, allowing the mating component to rotate relative to the shaft and stationary component. A sheath was 3D-printed to mount to the mating component, shown as pink in Figure 2.8. The clock-spring is installed within the sheath (space outlined in light blue in Figure 2.8), with the inner radius attached to the aluminum shaft, and the outer radius attached to the 3D-printed sheath. The tendon is then wrapped around outside of the sheath. A spring washer is included on the aluminum shaft in between the stationary and rotational components of the OTS electro-magnet clutch. This spring washer is strong enough to keep the two components separated when the clutch is off for minimum friction, but weak enough to be compressed when the clutch is on and allow for the normal force between the two components to create a large holding torque.

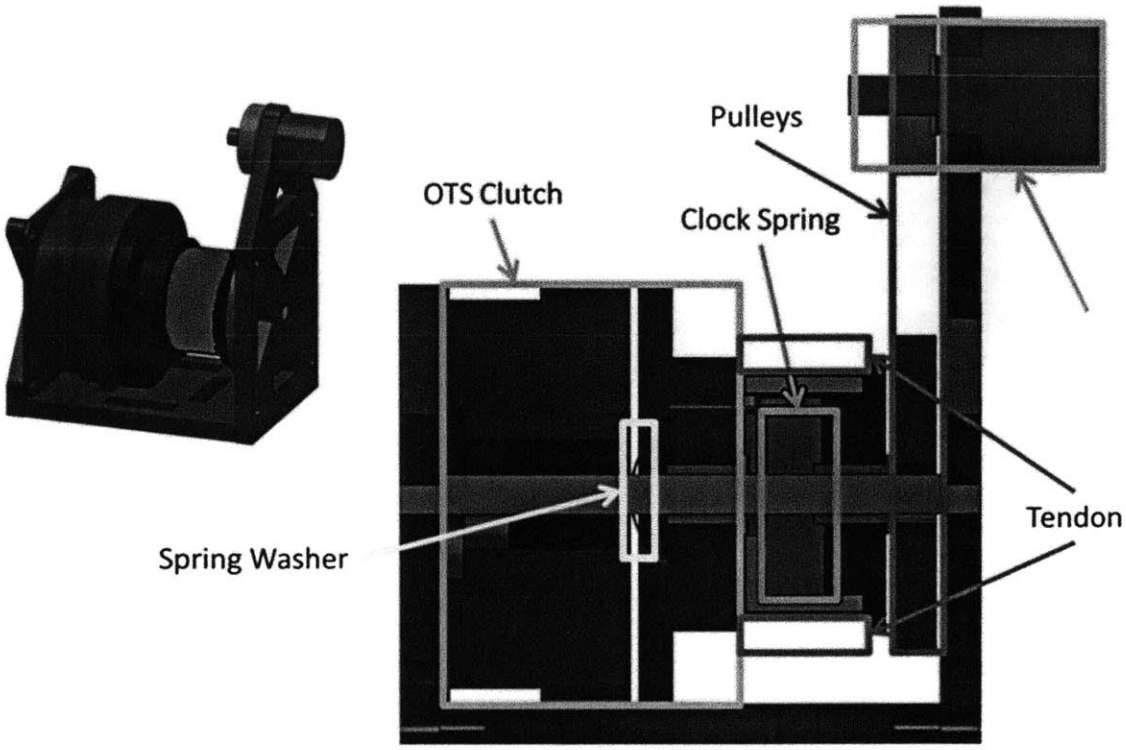

Figure 2.8 Cross-section of OTS clutch unit. The stationary component of the OTS clutch is shown in red, and the mating rotational component is shown in blue.

While the clutch is off, when the tendon is pulled and extended, the sheath and rotational mating component rotate relative to the stationary component and aluminum shaft. When the tendon is released, the clock-spring returns to its original position, retracting the extended tendon. Activating the clutch locks the rotational mating component and tendon wherever they are. Pulleys are used to translate the rotation of the mating component to a potentiometer, which could be used to measure the extension of the tendon. The fabricated prototype and clock-spring are shown in Figure 2.9.

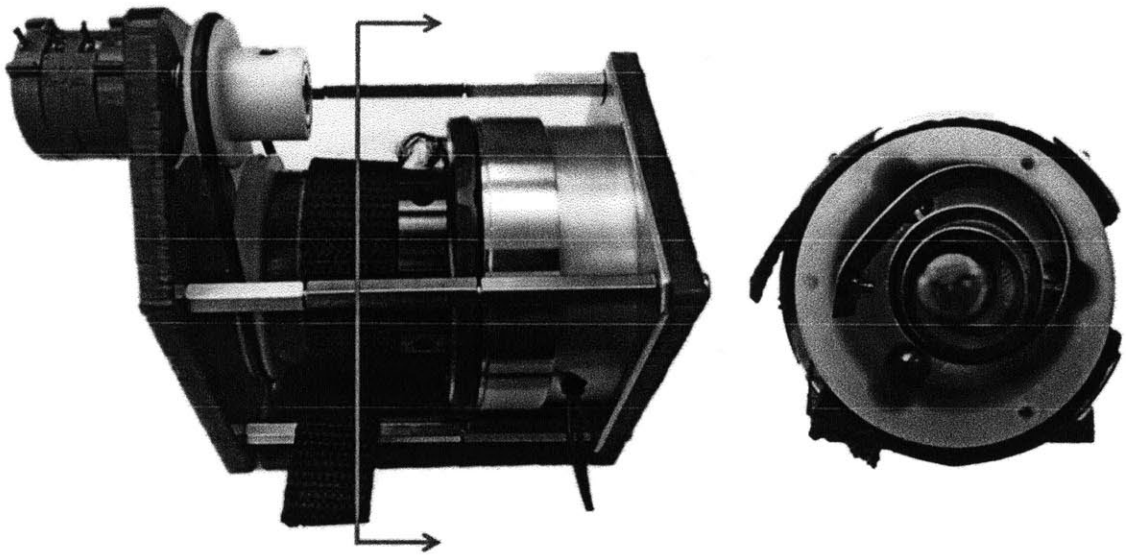

Figure 2.9 Close up image of the fabricated OTS clutch unit, and a cross-section showing the clock spring within.

2.6 Electro-Magnet Cone-Clutch Prototype

A second design and prototype for an electro-magnet clutch was attempted. The purpose of this prototype was to create a smaller electro-magnetic clutch than the OTS electro-magnet clutch through the use of a cone-clutch geometry. The interaction of a cup and cone in a cone-clutch yields a greater holding torque than the interaction of two plates for the same normal force. A cone-clutch diagram and its variables are shown in Figure 2.10.

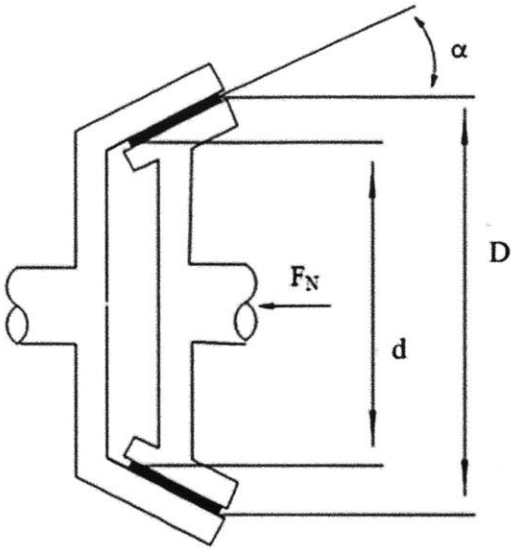

Figure 2.10 Schematic of a cone-clutch and the cup (left) and cone (right) interaction.

The holding torque, T, created by a cone-clutch is determined with the following expression[14]:

$$T = \frac{\mu F_N (D + d)}{4 \sin \alpha}, \qquad \text{Equation 2.2}$$

where μ is the coefficient of friction, F_N is the normal force between the cup and cone, D is the outer diameter of the cone, d is the inner diameter of the cone, and α is the angle of the cone.

In this design, the cone is the electro-magnet and the cup is the mating ferromagnetic surface. The normal force within the cone-clutch is created by the electro-magnet. Finite Element Method Magnetics (FEMM) was used to design the electro magnet. Figure 2.11 shows the FEMM analysis of the proposed electro-magnet. The force the electro-magnetic cone applies on the cup is about 245 N, which translates to a holding torque of about 4.25 Nm.

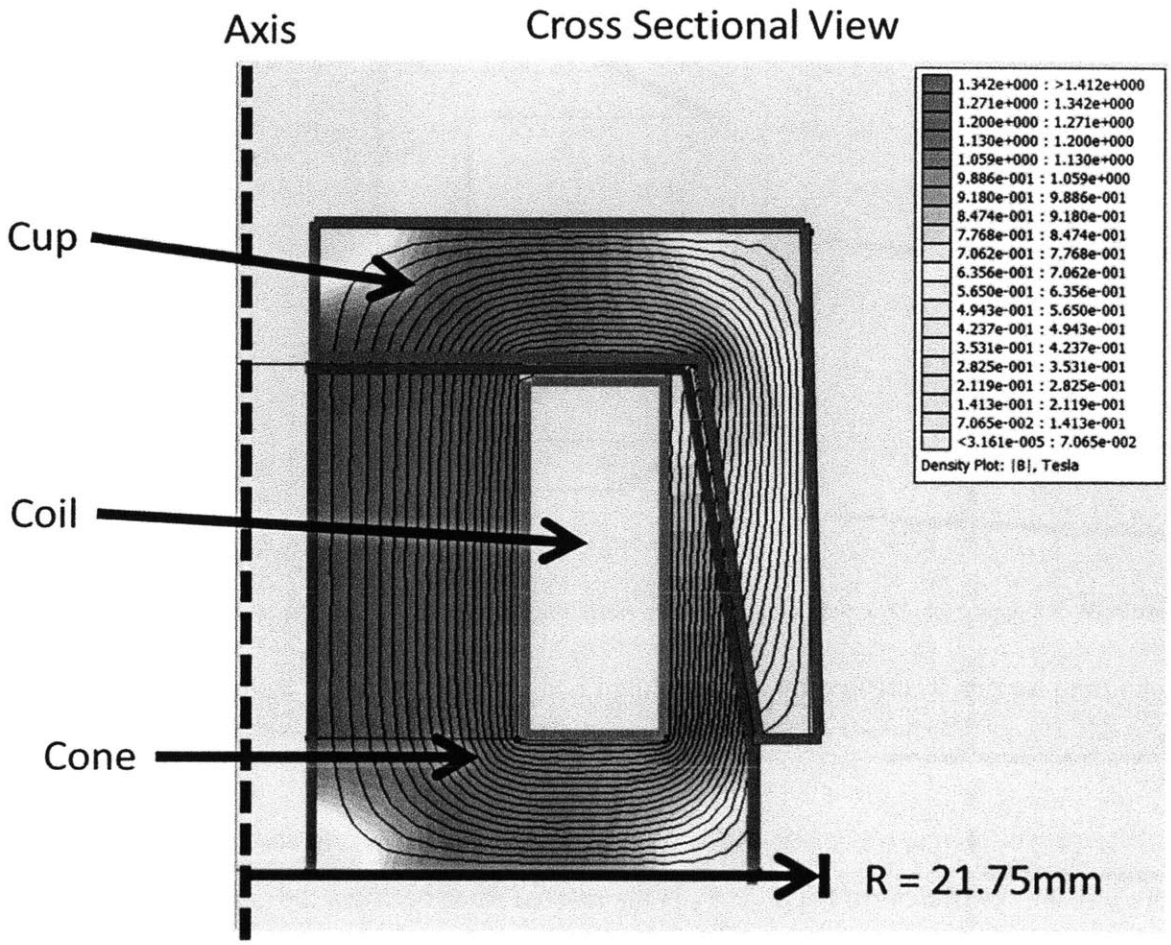

Figure 2.11 FEMM of cross section of designed electro-magnet. The normal force in this model is about 245 N, which yields a holding torque of about 4.25 Nm.

The design of the clutch unit is similar to that of the OTS electro-magnet clutch and is shown in Figure 2.12. The cone (red) and axis (yellow) are stationary, and the cup and sheath (blue and cyan) are allowed to rotate. The clock-spring within the sheath applies a restorative force on the cup sheath. When the electro-magnet is operated, the cup and sheath can no longer rotate and are locked.

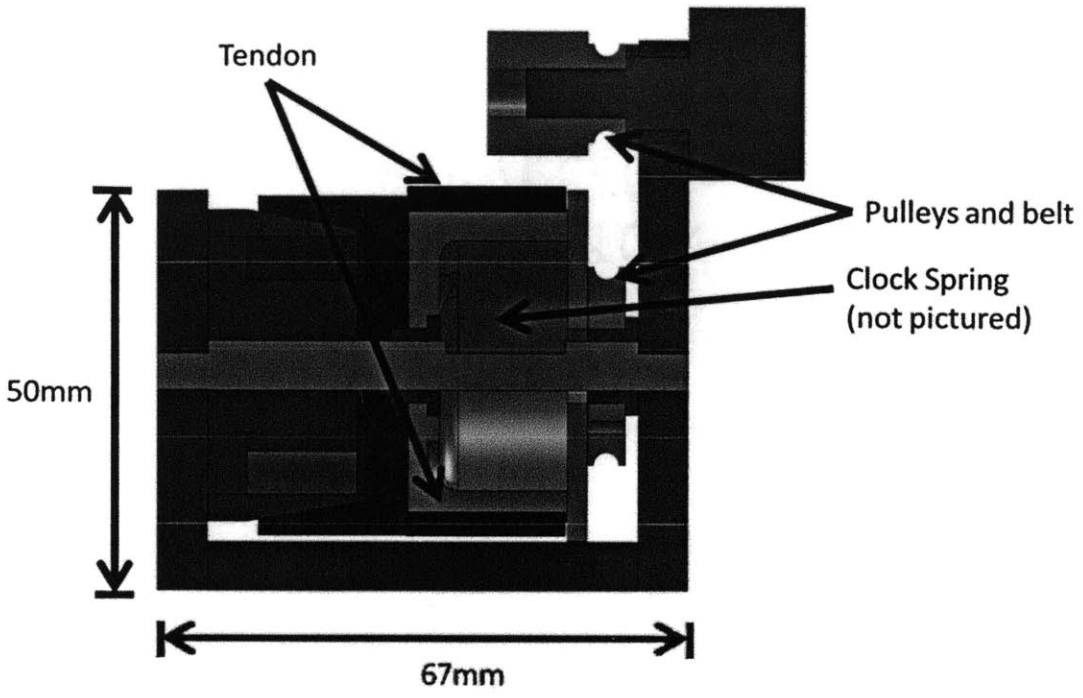

Figure 2.12 Cross-section of electro-magnet cone-clutch unit. The stationary component of the clutch is shown in red, and the mating rotational component is shown in blue.

A fabricated electro-magnet cone-clutch is shown in Figure 2.13 and a fabricated cone-clutch unit is shown in Figure 2.14.

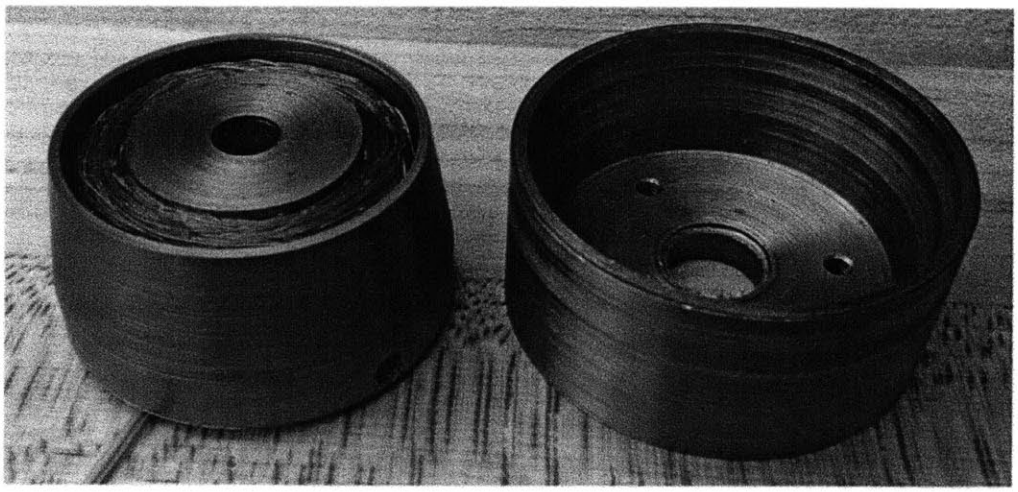

Figure 2.13 Fabricated electro-magnet cone-clutch. The electro-magnetic cone is on the left, and the mating cup is on the right.

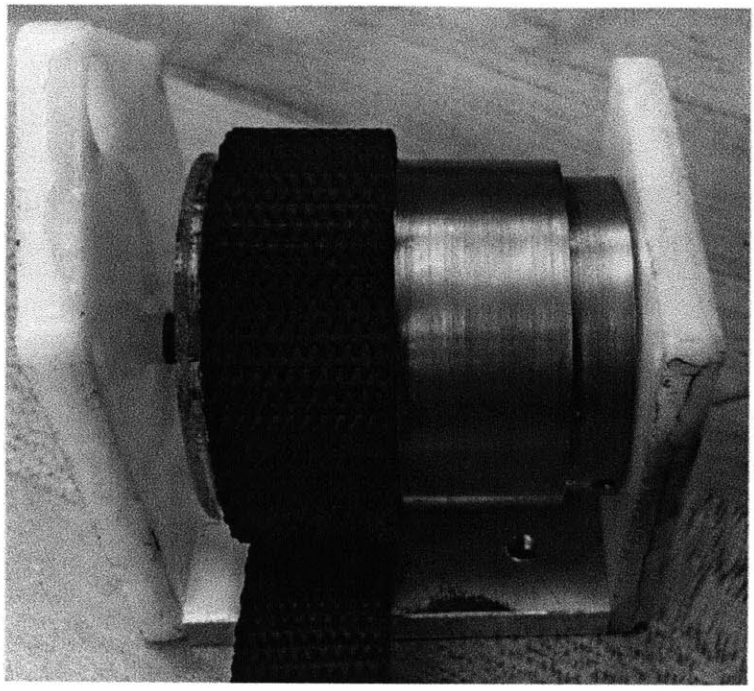

Figure 2.14 Assembled cone-clutch unit. When pulled, the tendon unwraps, but when the tension is removed, the tendon is retracted.

Testing of the electro-magnet cone-clutch yielded a holding torque of about 1 Nm, a quarter of the expected 4.25 Nm. The holding torque achieved in a cone clutch is highly dependent on the surface finish of the mating surfaces. Due to the manufacturing process (turning the surfaces on a manual lathe), the mating surfaces were not smooth enough to ensure the proper contact. Future prototypes could be improved by turning the components on a CNC lathe.

2.7 Wiring and Control

Footswitches from B & L Engineering (Figure 2.15) are used within the combat boots to sense when a food is bearing weight. Each footswitch has 4 sensors built in, a sensor at the heel, at the 1st and 5th metatarsals, and at the toes, to allow for distinction in weight distribution.

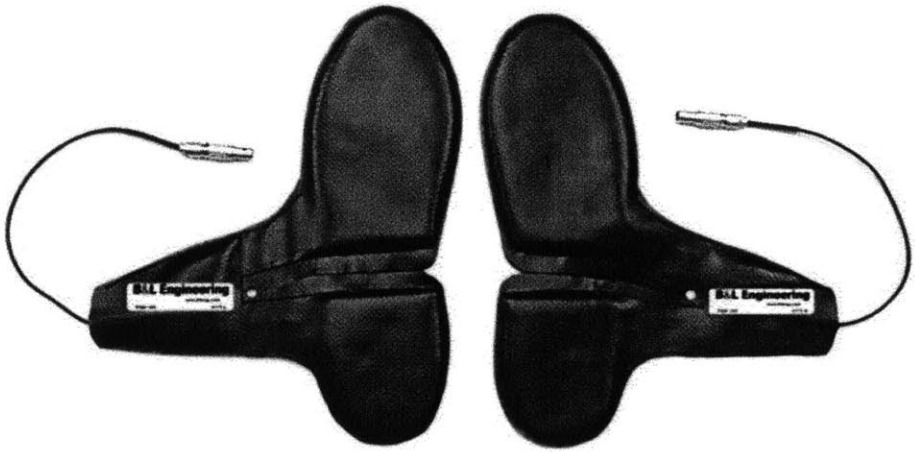

Figure 2.15 Footswitches from B & L Engineering. Footswitches have sensors at the heel, 1st and 5th metatarsal, and toes. The connectors used are 5-pin LEMO connectors.[15]

Another researcher in the lab designed and assembled a control box for use with the exotendon suit, shown in Figure 2.16. The box houses an mbed microcontroller and an XBee wireless antenna. The controller is written and transmitted to the microcontroller via the terminal emulator Tera Term. Feedback from the footswitches is used to control the timing of the clutch.

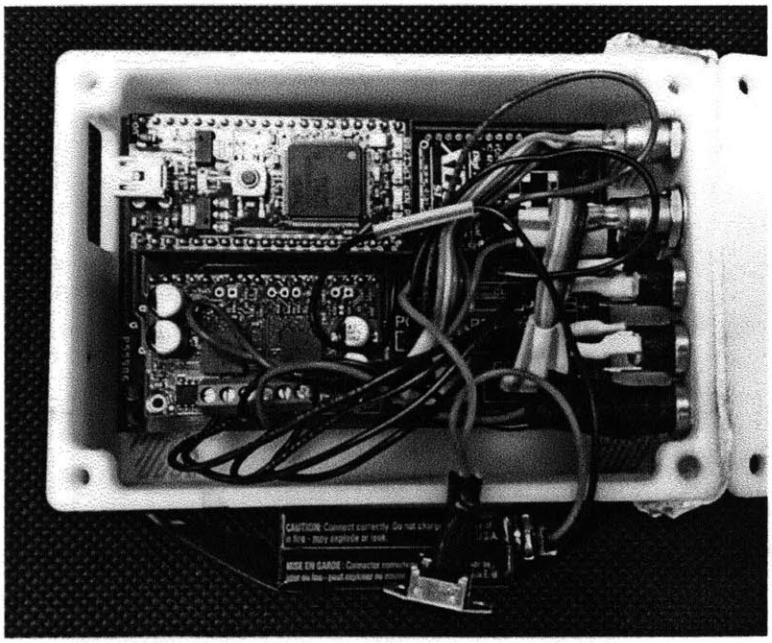

Figure 2.16 Control box housing the mbed microcontroller (Datasheet included in the Appendix).

The controller is powered by a 9 V battery, and the clutches are powered by two 12 V LiPo batteries.

2.8 Full Suit

Due to the poor results of the electro-magnet cone-clutch, the OTS electro-magnet clutch was used during experimental tests with subjects. The full suit and testing setup are shown on a subject in Figure 2.17. The subject is wearing all of the components of the exo-suit, including the rucksack and COSMED system, discussed in Chapter 3.

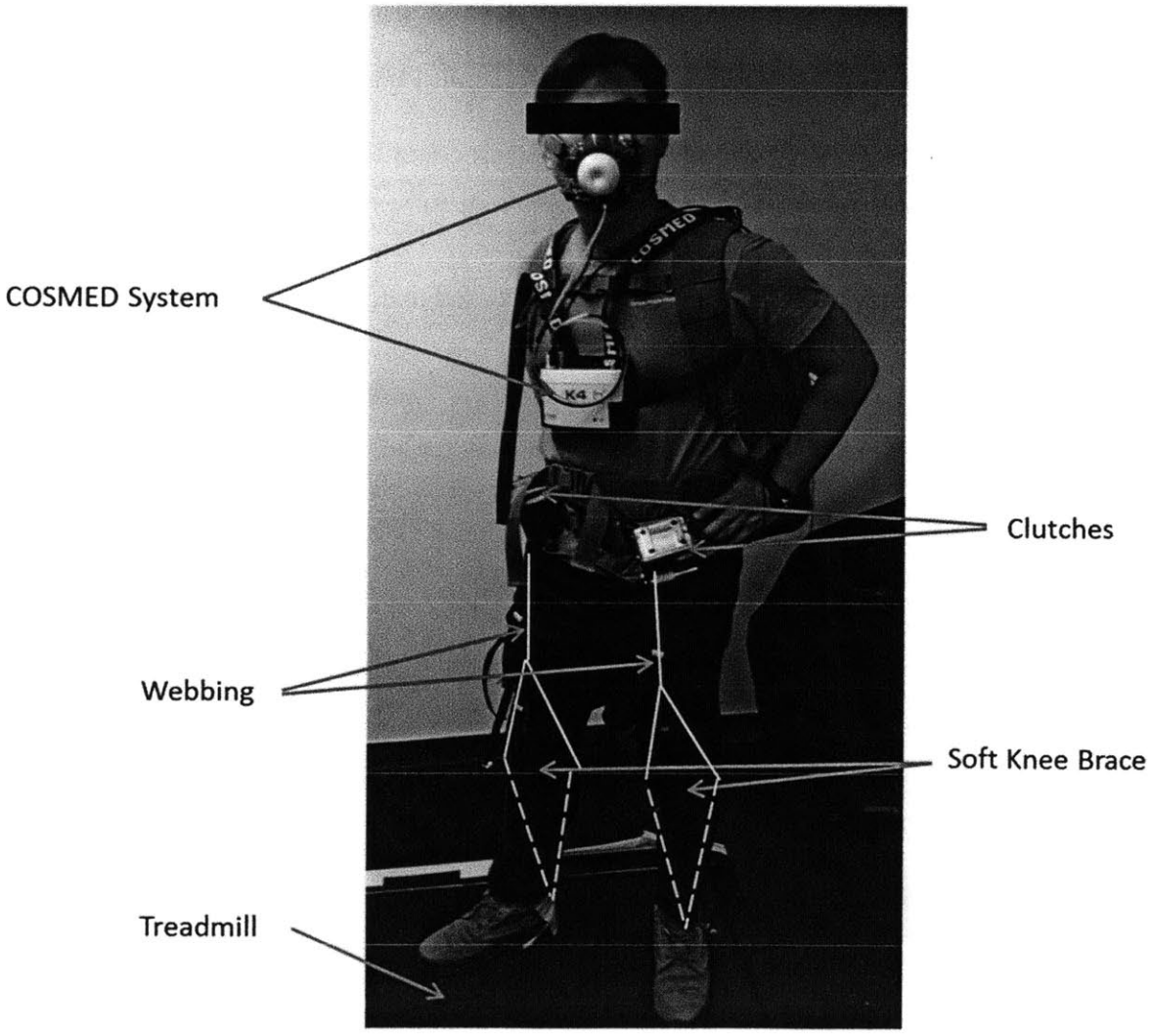

Figure 2.17 Subject with the exotendon suit and COSMED system donned.

3 Experimental Design and Results

Testing of the exotendon suit on a Bertec Fully Instrumented Treadmill (Bertec FIT) was accomplished at the Wyss Institute for Biologically Inspired Engineering's Motion Capture Laboratory (Figure 3.1). Five novice subjects performed, wearing a pair of military combat boots and carrying a standard issue MOLLE rucksack (Modular Lightweight Load-carrying Equipment) with a 20 kg load, both shown in Figure 3.2. Testing for each subject followed similar protocols, and metabolic power data and surface electromyograms (sEMG) were collected during testing with a COSMED K4b2 system and a Delsys Trigno system, respectively.

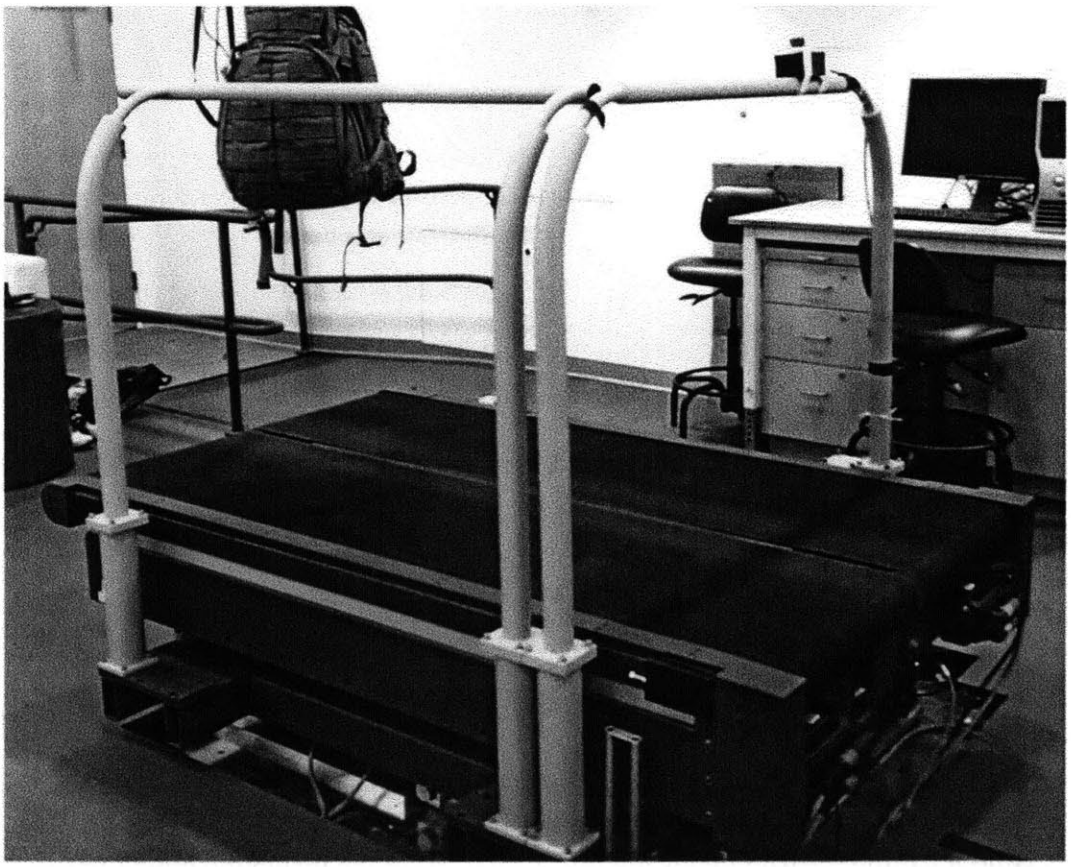

Figure 3.1 Bertec FIT treadmill used for the experiments. A safety harness is attached to the rucksack during testing, and an emergency stop button is at hand for the subject, should he or she ever feel uncomfortable.

Figure 3.2 An example of a military combat boot and MOLLE pack used by each subject during experimental testing.

3.1 Protocol

The subjects ranged in age from 23-28, with a mean height of 176.2 cm and a mean weight of 73.3 kg. Every trial was performed at a treadmill speed of 1.25 m/s. Each subject participated in six trials: two trials in street clothes; two trials with the exosuit donned but unpowered; and two trials with the exosuit donned and powered.

A sample protocol followed is shown in Table 3.1. Every subject's first and last trials were done in street clothes. Ideally, metabolic power measurements of the identical first and last trials should be similar. If the measurements are not similar, all of the metabolic power measurements need to be adjusted. Subjects wear athletic shorts, combat boots, and carry the rucksack during these two trials.

The exosuit is worn during the four middle trials. These trials are any combination of two active suit trials, and two passive suit trials. Each trial is about 8 minutes long, separated by 5 minute rest periods.

Table 3.1 A sample protocol used during subject testing at the Wyss Institute

Trial	Test Condition	Time (minutes)
1	Street Clothes	8
	Rest	5
2	Passive Exosuit	8
	Rest	5
3	Active Exosuit	8
	Rest	5
4	Active Exosuit	8
	Rest	5
5	Passive Exosuit	8
	Rest	5
6	Street Clothes	8

A subject performing the experiment is shown in Figures 3.3 and 3.4 from the front and side.

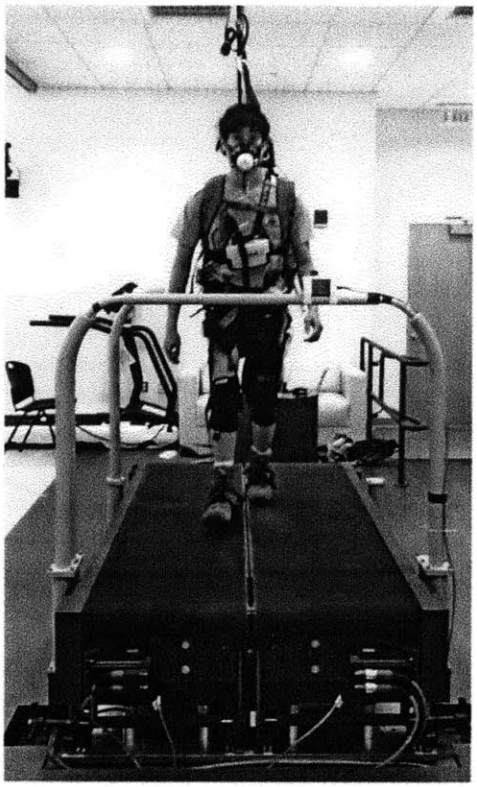

Figure 3.3 Front view of subject participating in the experiment.

Figure 3.4 Side view of subject participating in the experiment.

3.2 Collection and Analysis of Metabolic Power Data

A COSMED K4b2 system (Figure 3.5) is used in every trial to measure pulmonary gas exchange. This portable metabolic measurement system is worn by the subject. A mask covers the subject's nose and mouth and a harness is worn to carry the portable system.

Figure 3.5 Portable COSMED K4b2 system and mask worn by subjects during experimental testing.[16]

Energy expenditure can be estimated with the COSMED K4b2 system by measuring pulmonary gas exchange. In particular, VO2 and VCO2 measurements are considered. VO2 and VCO2 refer to the rate at which one inhales oxygen and exhales carbon dioxide, respectively. During load carriage, the volume of oxygen and carbon dioxide exchanged increases and plateaus, as shown in Figure 3.6.

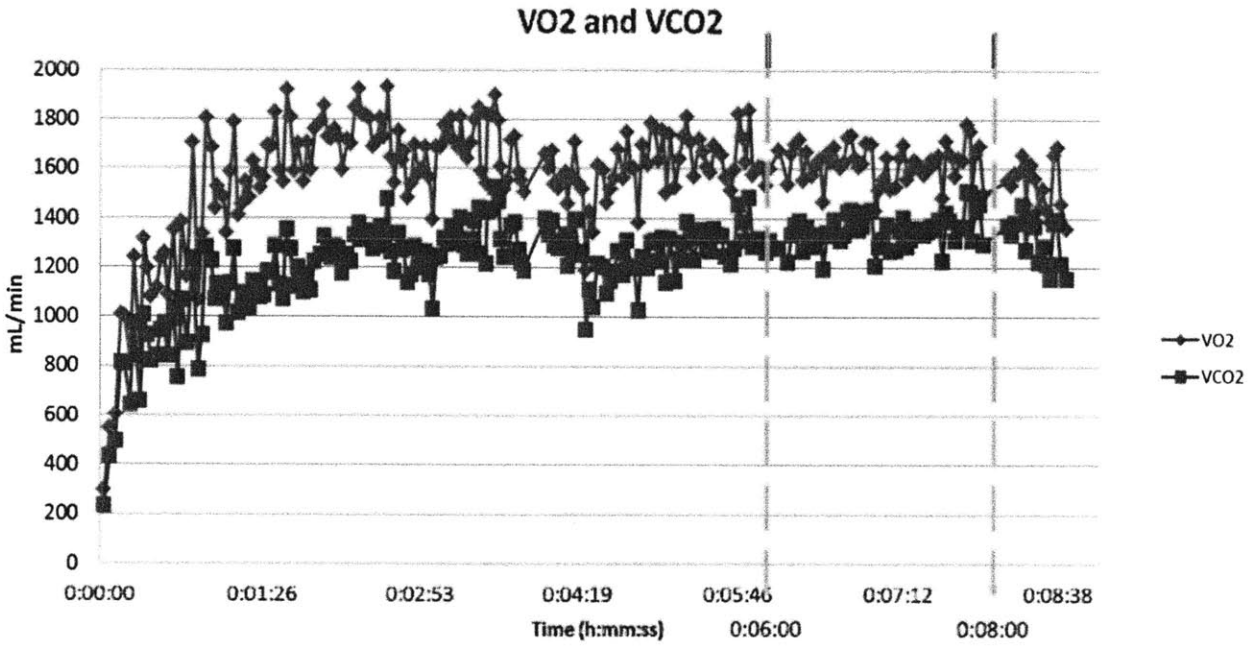

Figure 3.6 VO2 and VCO2 measurements of a subject during load carriage, taken over a trial about 8 minutes long. The average values of VO2 and VCO2 are taken from a 2 minute segment between the 6th and 8th minute for metabolic power calculations.

Subject trials are 8 minutes to allow for VO2 and VCO2 measurements to plateau. A 2 minute segment of the plateau is averaged and used to calculate metabolic power. For a trial, the metabolic power is calculated using the following equation,[17]

Equation 3.1

where *VO2* and *VCO2* are the average VO2 and VCO2 measurements over a time period *t*.

Results and Discussion

To compare results between subjects, the metabolic power is normalized with the subjects' weights, and repeated trials were averaged. A summary of the results is shown in Table 3.2 and Figure 3.7.

Table 3.2 Metabolic power, normalized by weight, for the three conditions tested.

Subject	Metabolic Power (W/kg)			% Increase from Passive to Active Conditions
	Street Clothes	Passive	Active	
1	N/A	5.90	6.09	3.34
2	6.92	7.34	7.11	-3.13
3	6.80	6.75	6.85	1.42
4	5.63	5.98	5.68	-5.06
5	6.81	7.41	7.11	-4.07

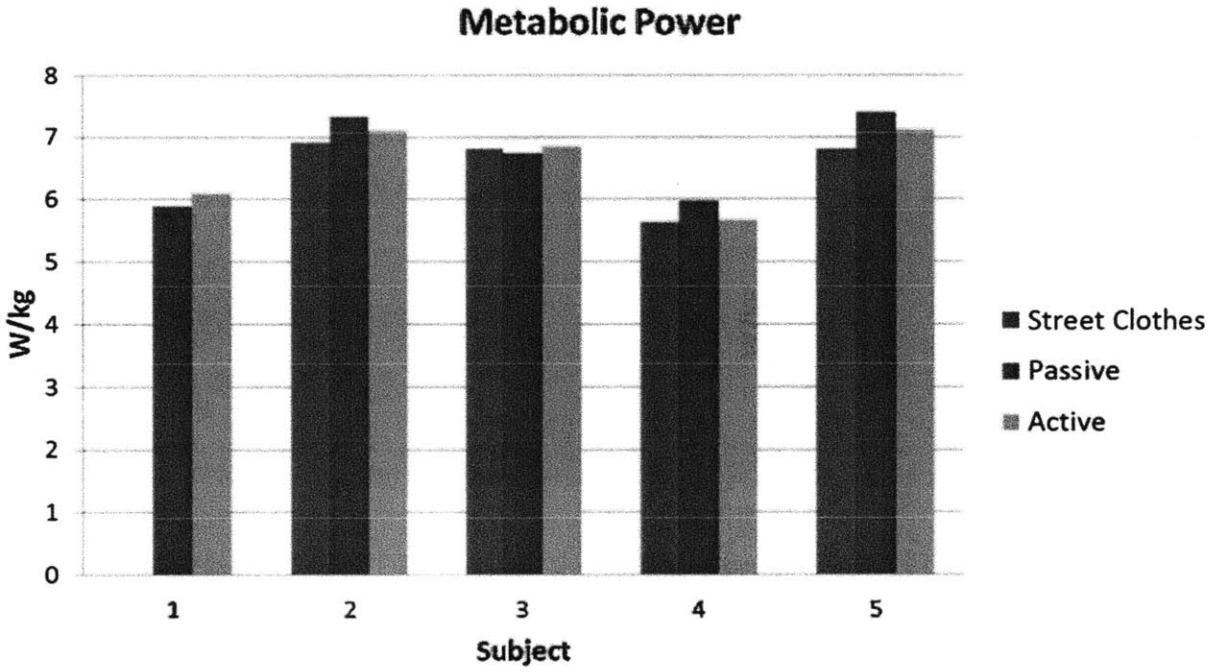

Figure 3.7 Metabolic power, normalized by weight, for the three conditions tested.

The results of these tests do not show a significant effect of activating the exosuit. Metabolic power results from trials where the suit was powered were within ±5% of the results from trials where the suit was worn but unpowered. No clear trend is visible. However, only 5 tests were executed. More subjects and more trials could possible allow a trend to be seen if there is one.

3.3 Collection and Analysis of Electromyography

Surface electromyogram (sEMG) data was collected during testing with a Delsys Trigno system. Four sEMG sensors were used on one of each subjects' legs to measure the muscle activation of the gastrocnemius lateralis, tibialis anterior, bicep femoris, and vastus medialis muscles. Placement of the sensors is shown in Figure 3.8.

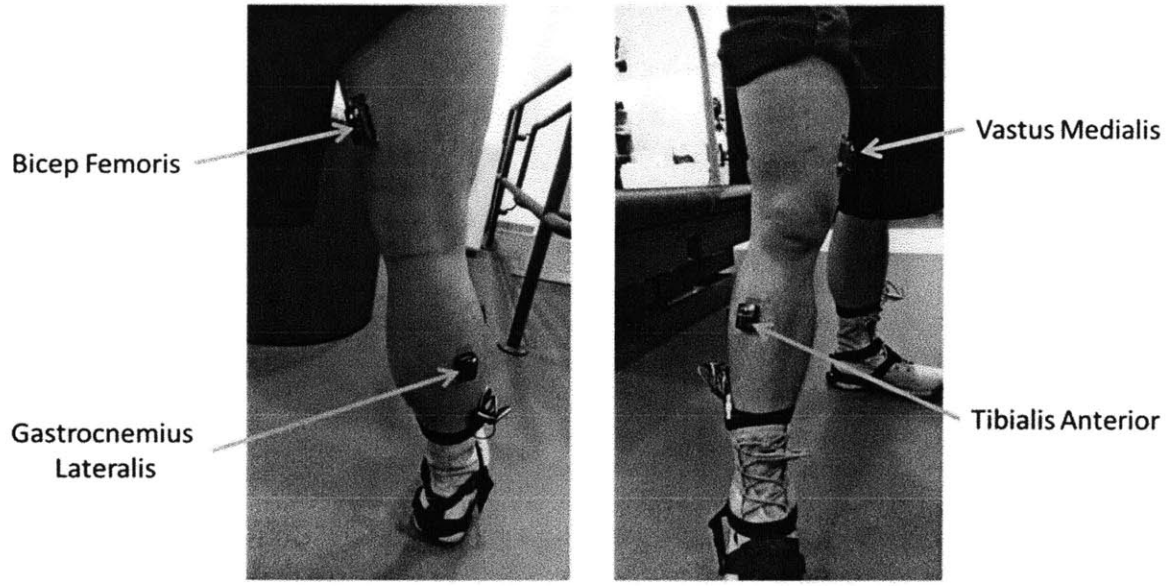

Figure 3.8 Placement of sEMG sensors on a subject's leg.

The sEMG sensors measure the electrical signals that muscles output during activation. For best results, the skin on which the sensors are placed should be shaved and cleaned, removing dead skin cells. This yields a lower skin impedance at the points of contact of the electrodes. In this study, none of the participants opted to have their legs shaved. Figure 3.9 shows a sample raw EMG recording taken of the gastrocnemius lateralis during this study.

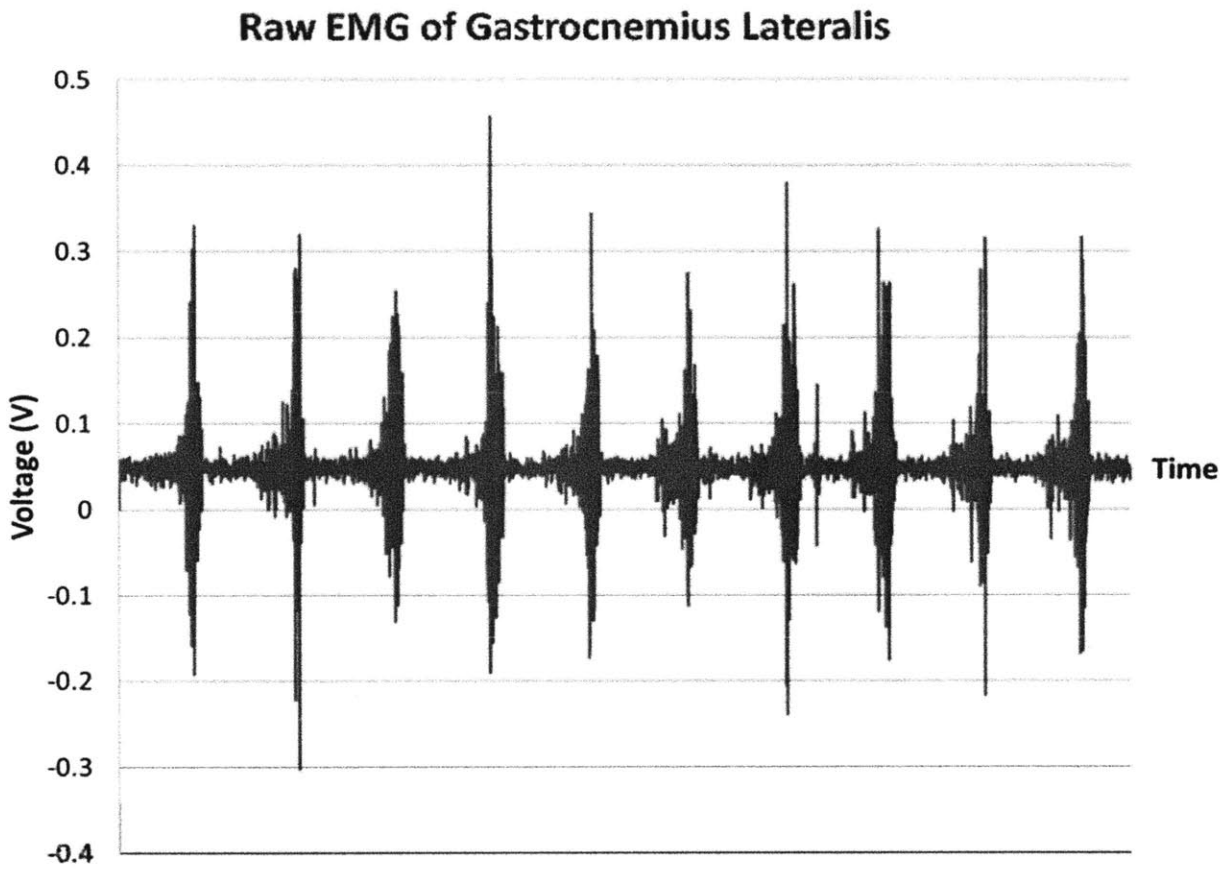

Figure 3.9 Raw EMG data gathered from a sEMG sensor on the gastrocnemius lateralis.

Due to the large amount of noise in the raw measurement data, in order to make comparisons between different trials, the data is normalized and rectified. Because of the random nature of EMG signals, the data must be digitally smoothed once the data is normalized and rectified. The most common method of smoothing is by a root mean square (RMS) smoothing algorithm, which is used in this study.[18] The RMS smoothing is achieved by calculating the square root of the mean of the sum of squares of a specified envelope around each point:

Equation 3.2

For most EMG application, an envelope of 20 – 500 ms is used.[19] For this study, an envelope of 150 ms was used. Figure 3.10 shows a portion of the data from Figure 3.9 normalized and rectified in blue, and the result of the smoothing algorithm in red.

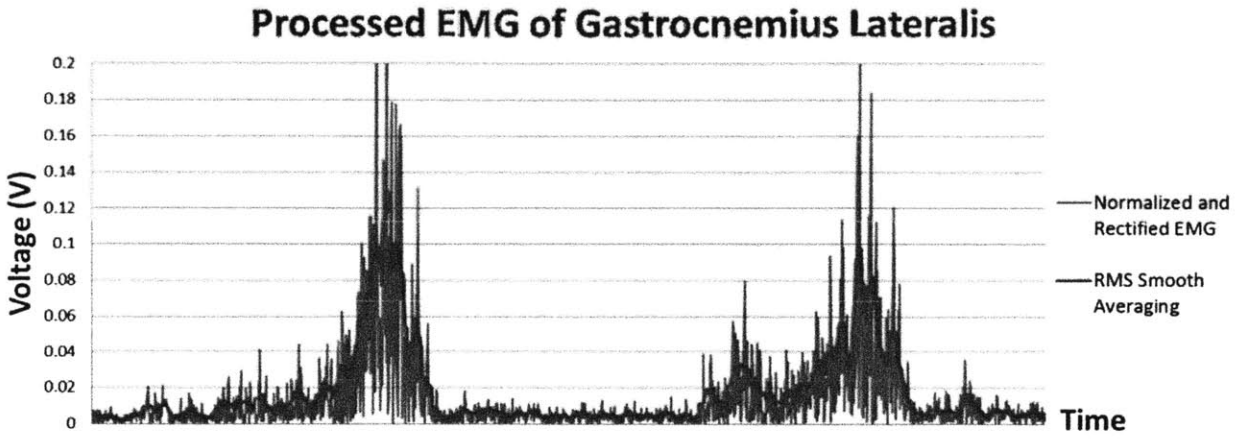

Figure 3.10 Processed EMG data gathered from a sEMG sensor on the gastrocnemius lateralis. First, the data is normalized and rectified (blue), then it is smoothed using a RMS smooth averaging algorithm.

The amplitude mean is used to quantitatively compare the EMG measurements of different trials for the same muscle. The means are calculated during the time periods of muscle activation, as shown in Figure 3.11. In this study, the calculated means for a two minute period of the trial (between minutes 6 and 8, as during metabolic power calculations) are averaged and compared.

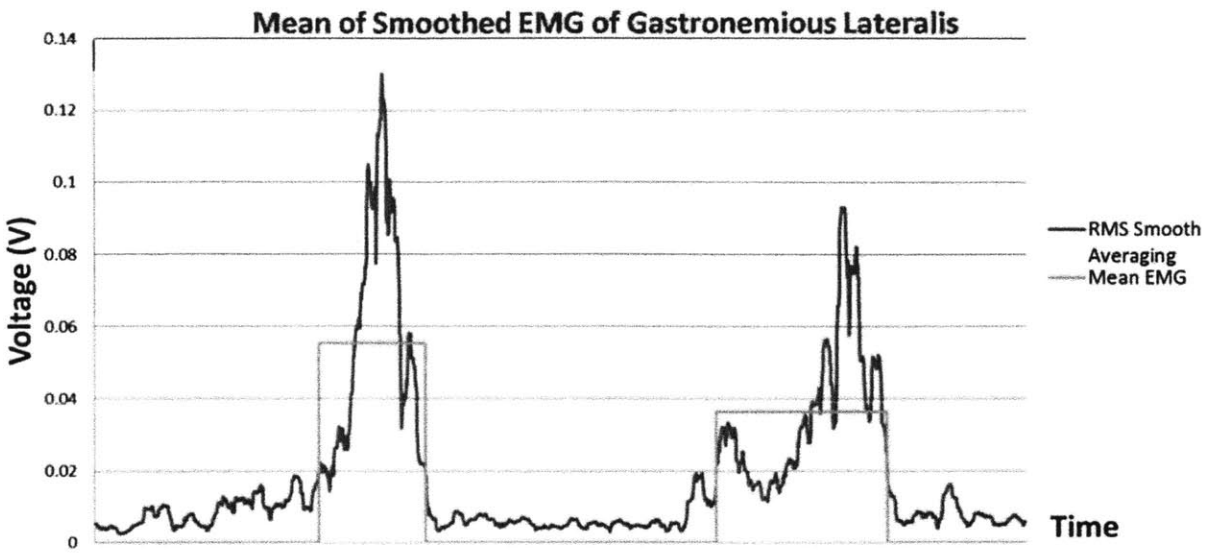

Figure 3.11 Processed EMG data gathered from a sEMG sensor on the gastrocnemius lateralis is shown in red. The mean voltage amplitudes for muscle activations are shown in green.

Results and Discussion

EMG measurements between different muscles and different subjects are not easily compared, so only relative measurements between passive and active conditions are compared in this study. A summary of the results is shown in Tables 3.3 – 3.6 and Figures 3.12 – 3.15.

Table 3.3 Mean EMG values for gastrocnemius lateralis muscles, for the three conditions tested.

Subject	Mean EMG (mV)			% Increase from Passive to Active Conditions
	Street Clothes	Passive	Active	
1	N/A	59.0	59.2	0.364
2	46.8	47.9	48.8	1.71
3	93.3	93.3	77.7	-16.7
4	40.3	44.0	42.2	-4.20
5	78.5	75.8	68.5	-9.70

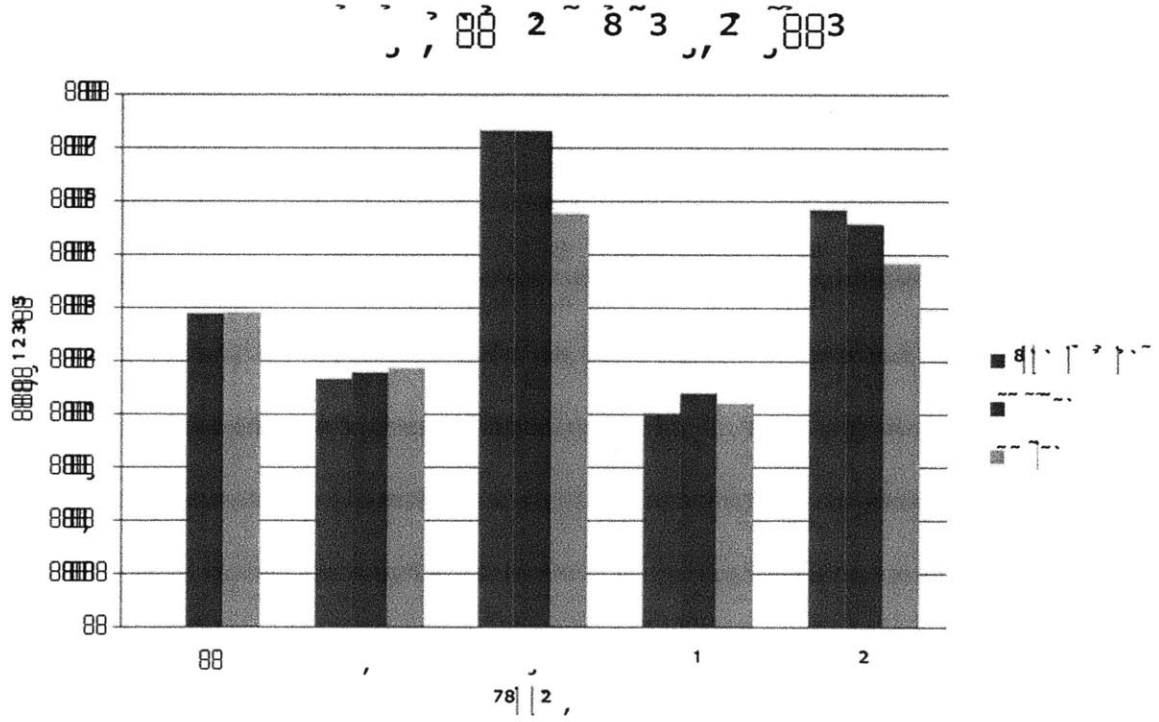

Figure 3.12 EMG values for the gastrocnemius lateralis muscles, for the three conditions tested.

Table 3.4 Mean EMG results for tibialis anterior muscles, for the three conditions tested. The sEMG sensor used on Subject 1 for the tibialis anterior measurements experienced excessive noise that could not be isolated. The data from this sensor was not used in the calculations for the results.

Subject	Mean EMG (mV)			% Increase from Passive to Active Conditions
	Street Clothes	Passive	Active	
1	N/A	N/A	N/A	N/A
2	56.7	64.4	59.5	-7.69
3	54.7	53.3	52.2	-1.97
4	53.5	54.9	59.4	8.21
5	93.7	82.7	95.3	15.4

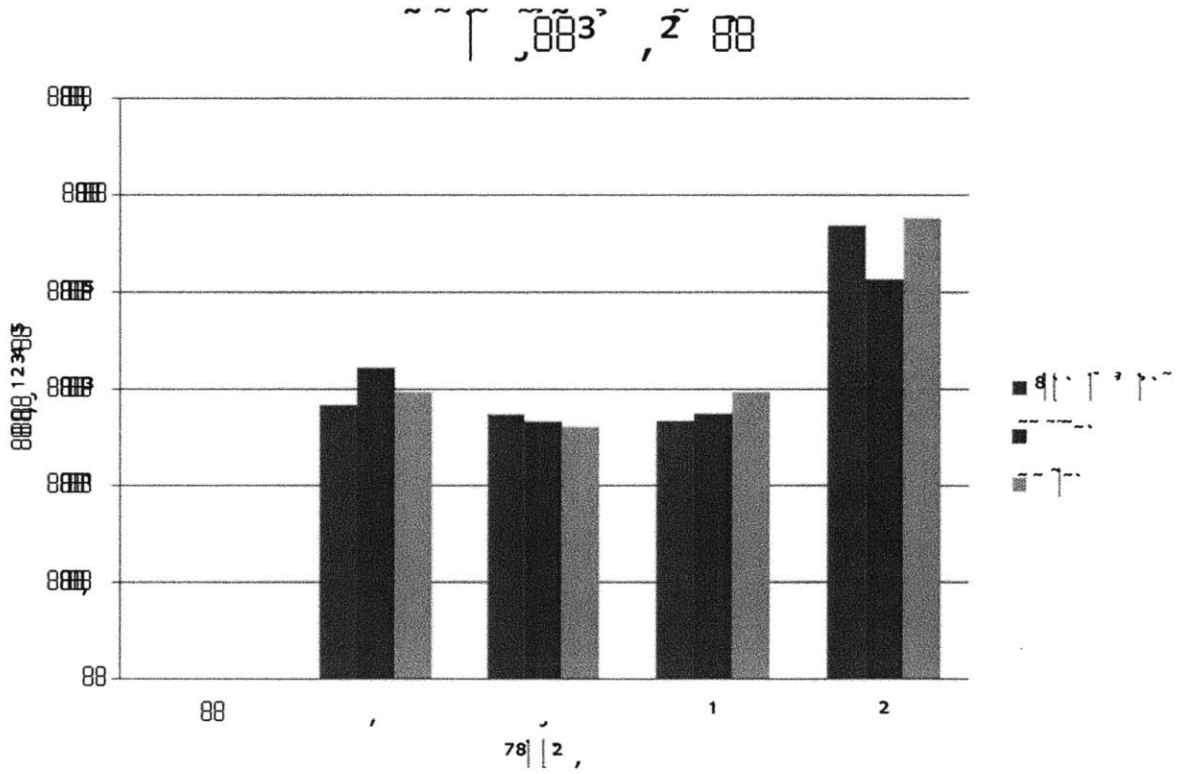

Figure 3.13 EMG values for the tibialis anterior muscles, for the three conditions tested. The sEMG sensor used on Subject 1 for the tibialis anterior measurements experienced excessive noise that could not be isolated. The data from this sensor was not used in the calculations for the results.

Table 3.5 Mean EMG results for bicep femoris muscles, for the three conditions tested.

Subject	Mean EMG (mV)			% Increase from Passive to Active Conditions
	Street Clothes	Passive	Active	
1	N/A	48.1	42.7	-11.4
2	26.7	27.3	25.8	-5.59
3	28.6	26.1	25.8	-1.06
4	39.0	39.4	37.9	-3.85
5	82.0	75.7	80.9	6.81

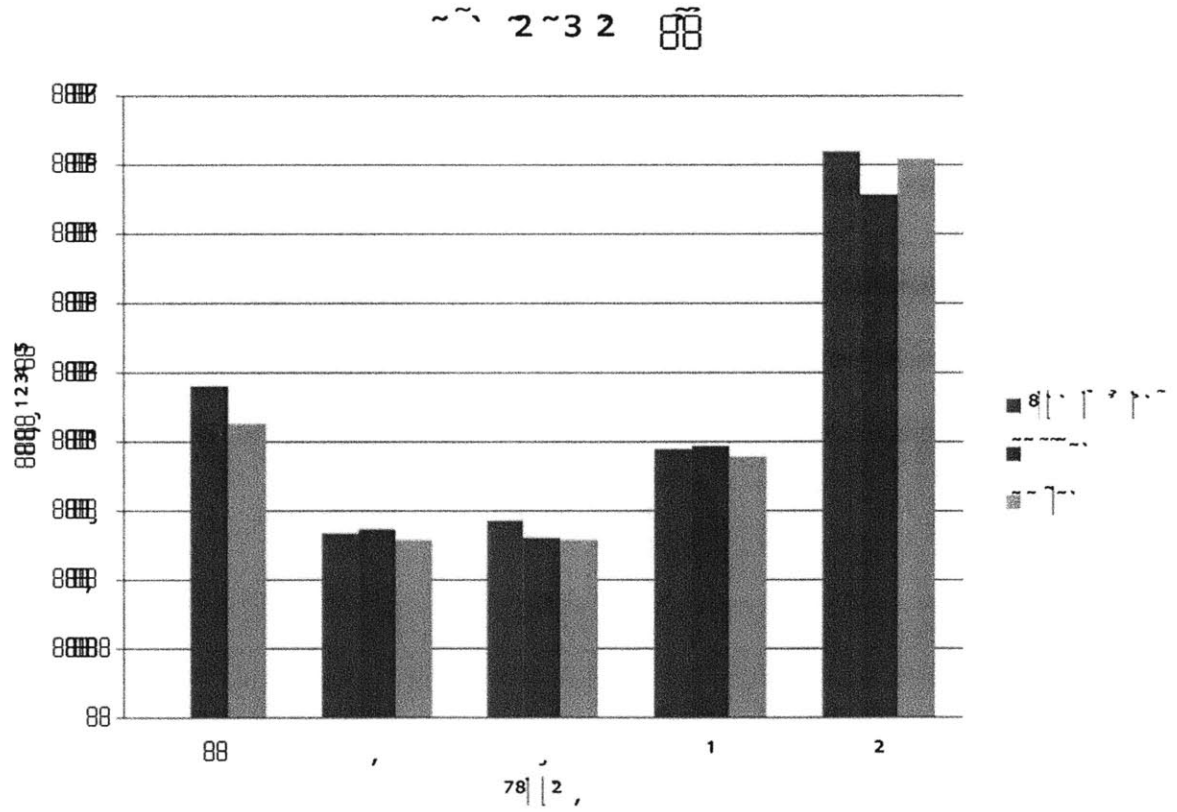

Figure 3.14 EMG values for the bicep femoris muscles, for the three conditions tested.

Table 3.6 Mean EMG results for vastus medialis muscles, for the three conditions tested. The sEMG sensor used on Subject 3 for the vastus medialis measurements experienced excessive noise that could not be isolated. The data from this sensor was not used in the calculations for the results.

Subject	Mean EMG (mV)			% Increase from Passive to Active Conditions
	Street Clothes	Passive	Active	
1	N/A	33.6	35.6	6.04
2	43.8	44.1	38.6	-12.6
3	N/A	N/A	N/A	N/A
4	46.4	45.1	44.4	-1.56
5	57.8	54.4	53.3	-1.94

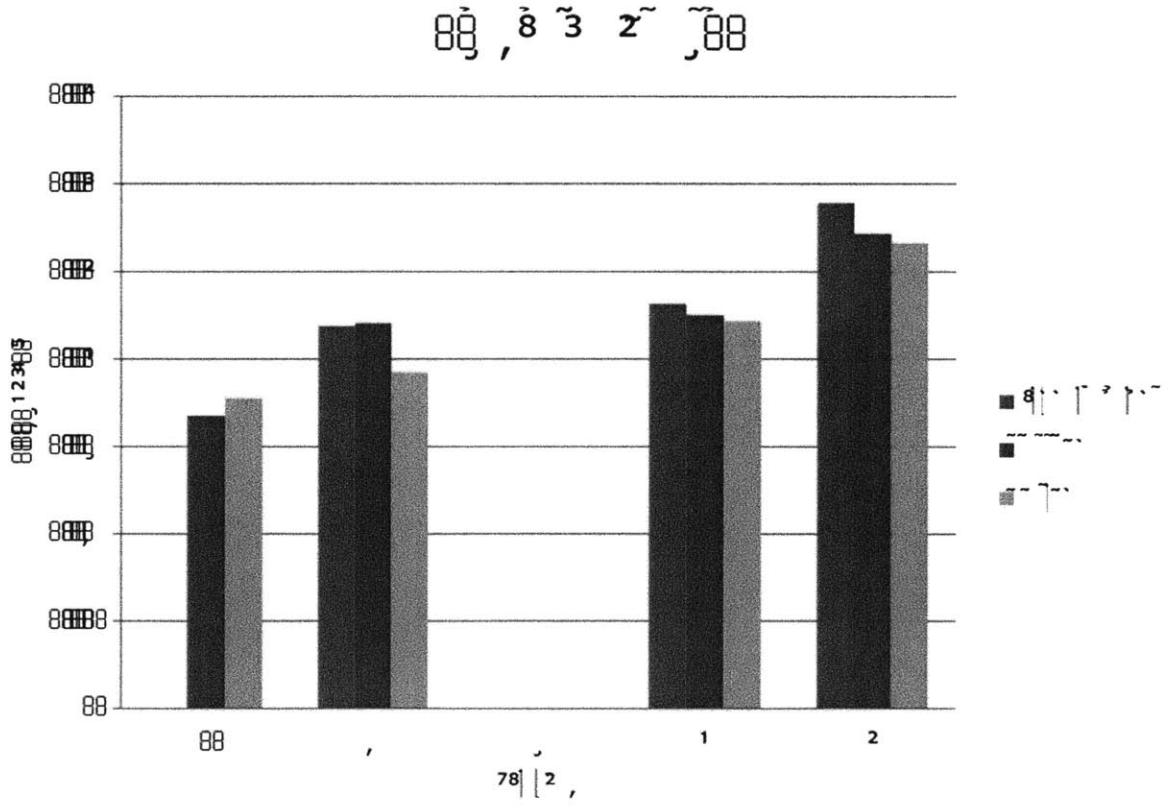

Figure 3.15 EMG values for the vastus medialis muscles, for the three conditions tested. The sEMG sensor used on Subject 3 for the vastus medialis measurements experienced excessive noise that could not be isolated. The data from this sensor was not used in the calculations for the results.

The results of these tests are highly variable and do not show a significant effect in activation of the exosuit. Half of the mean EMG amplitude results from trials where the suit was powered were within ±5% of the results from trials where the suit was worn but unpowered. An additional 5 of the 18 sets had powered systems within ±10%, while the remaining 4 results are within ±17%. The results are both positive and negative, with no visible trend.

The sEMG sensor placement was not ideal in many cases, which had an effect on the results obtained. For some subjects, the sensors on the upper leg would be brushed by the subject's athletic shorts. This phenomenon made the results from the vastus medialis sEMG sensor on Subject 3 unusable, and may have also skewed the other results. In addition, none of the subjects opted to shave patches of their legs to allow for better conductivity between the sEMG electrodes and the subjects' muscles, so the results were not of the best quality. These factors, and other possible noise sources, are likely the cause for the highly variable results obtained for the EMG portion of the experiment.

4 Conclusions and Future Work

The goal of this thesis was the design, development, and evaluation of a lightweight, exotendon suit for load carriage.

A simple exotendon suit architecture was designed and implemented, consisting of two knee braces, a length of polypropylene tendon, a belt, two electro-magnet clutches, and a control box. The knee radius of the tendon routing was optimized for comfort during testing and off-the-shelf knee braces were modified for a radius of zero. The soft architecture allows the user to move freely, as it does not impede the wearer's natural motions. Two actuation strategies were considered, EPMs and electro-magnets. EPM clutches were dismissed due to complicated power electronics. Two pairs of electro-magnet clutches were designed and prototyped (OTS clutch and cone-clutch). The OTS electro-magnet clutches were used during experimental testing due to their higher holding torques.

Metabolic power testing and EMG data collecting was performed at the Wyss Institute Motion Capture Lab on five subjects for three different conditions: street clothes, exosuit worn but unpowered, and exosuit worn and powered. Results of the tests were inconclusive. There was no significant evidence that powering the exosuit has a positive or negative effect on the wearer's energy usage.

In order to determine the effect the exotendon suit has on human walking, more testing needs to be performed. In this round of experiments, five subjects were used. Another round of experiments with double the subjects would more likely highlight a trend. Another consideration to take into account while designing further experiments is the effect of learning on human energy expenditure. In the study of their exoskeleton, Sawicki and Ferris determined that the

metabolic energy usage measured decreased in users over three sessions on three different days.[10] This implies that for best results, the subjects should train in at least two sessions before taking data.

The major result of this thesis is the development of a platform and protocol for future experiments. Current exoskeleton research involving actuators at the ankle have not been successful in reducing metabolic energy due to the additional weight to the ankle. More effort is being put into systems where the actuators are located closer to the torso, minimizing the weight at the extremities. Wehner shows some promising results with their exosuit, with metabolic power of the active suit as low as metabolic power used walking without the suit.[20] The future of exoskeletons is headed towards light, flexible, low-power systems, and this thesis is working towards these new ideals.

References

[1] Kazerooni, H., Stegar, R., "The Berkeley lower extremity exoskeleton (BLEEX)." *J. Dyn. Syst. Meas. Control-Trans. ASME,* 128, 2006.

[2] Low, K. H., Liu, X. P., Goh, C. H., Yu, H. Y., "Locomotive control of a wearable lower exoskeleton for walking enhancement." *J. Vib. Control* 12, 2006.

[3] Ferris, D. P., Gordon, K. E., Sawicki, G. S., Peethambaran, A., "An improved powered ankle-foot orthosis using proportional myolectric control." *Gait & Posture,* Vol. 23, 2006.

[4] Pratt, J. E., Krupp, B. T., Morse, C. J., Collins, S. H., "The RoboKnee: An exoskeleton for enhancing strength and endurance during walking." *IEEE Int. Conf. Robotics and Automation*, New Orleans, LA, (IEEE Press) 2004.

[5] Ferris, D. P., Sawicki, G. S., Daley, M. A., "A Physiologist's perspective on robotic exoskeletons for human locomotion." *Int. J. Humanoid Robotics,* Vol. 4, No. 3, 2007.

[6] Norris, J. A., Granata, K. P., Mitros, M. R., Byrne, E. M., Marsh, A. P., "Effect of augmented plantarflexion power on preferred walking speed and economy in young and older adults." *Gait & Posture*, Vol 25, Issue 4, April 2007.

[7] Sawicki, G. S., Ferris, D. P., "Mechanics and energetics of level walking with powered ankle exoskeletons." *The Journal of experimental biology*, Vol. 211, May 2008.

[8] Lenzi, T., Zanotto, D., Stegall, P., Carrozza, S. K., Agrawal, M. C., "Reducing Muscle Effort in Walking through Powered Exoskeletons." *Proceedings of the 34th Annual International Conference of the IEEE EMBS,* San Diego, California. 28 August - 1 September, 2012.

[9] Browning, R. C., Modica, J. R., Kram, R. Goswami, A., "The effects of adding mass to the legs on the energetics and biomechanics of walking." *Med. Sci. Sports Exerc.* Vol. 39, 2007.

[10] Sawicki, G. S., Ferris, D. P., "Powered ankle exoskeletons reveal the metabolic cost of plantar flexor mechanical work during walking with longer steps at constant step frequency." *The Journal of experimental biology*, Vol. 212, January 2009.

[11] Knaian, A. N., "Electropermanent Magnetic Connectors and Actuators: Devices and Their Application in Programmable Matter." Diss. Massachusetts Institute of Technology, Cambridge, 2010.

[12] "Flanged Mounted Power-On Brakes." Stock Drive Products/Sterling Instruments. 2013. 1 August, 2013. sdp-si.com.

[13] "Spiral Torsion Springs." Springs & Things Incorporated. 2013. www.springsandthings.com.

[14] Shigley, Joseph and Charles Mischke. Mechanical Engineering Design. 6th ed. Boston: McGraw Hill, 2001.

[15] "Footswitches." B & L Engineering. 2013. www.bleng.com.

[16] "Cardiopulmonary Exercise Testing." COSMED Pulmonary Function Equipment. 2013. www.cosmedusa.com.

[17] Brockway, J. M., "Derivation of formulae used to calculate energy expenditure in man." *Hum. Nutr. Clin. Nutr.*, Vol. 41, No. 6, 1987.

[18] Basmajian, J. V., De Luca, C. J., "Muscles Alive: Their Function Revealed by Electromyography." Williams Wilkins, Baltimore 1985.

[19] Konrad, P., "The ABC of EMG: A Practical Introduction to Kinesiological Electromyography." Noraxon EMG & Sensor Systems. 2005.

[20] Wehner, M., Quinlivan, B., Aubin, P. M., Martinez-Villalpando, E., Baumann, M., Stirling, L., Holt, K., Wood, R., "A Lightweight Soft Exosuit for Gait Assistance." *IEEE International Conference on Robotics and Automation (ICRA),* Karlsruhe, Germany, May 6-10, 2013.

Appendix

Clutch Product Finder

Inch Inch Inch Inch Inch Inch Inch Inch Inch

SDP/SI — **Power-On Flange-Mounted Brakes**

Stock Drive Products/Sterling Instrument ■ Phone: 516-328-3300 ■ Fax: 516-328-8627

■ 24 VOLTS DC ■ ANTIBACKLASH WHEN ENERGIZED

■ ZERO DRAG WHEN DE-ENERGIZED

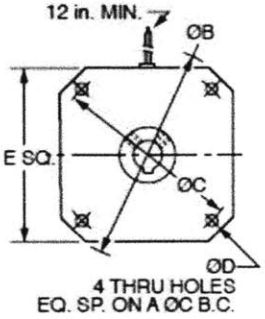

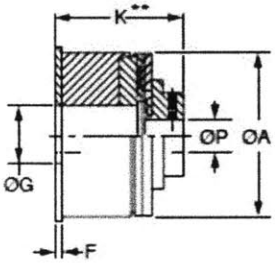

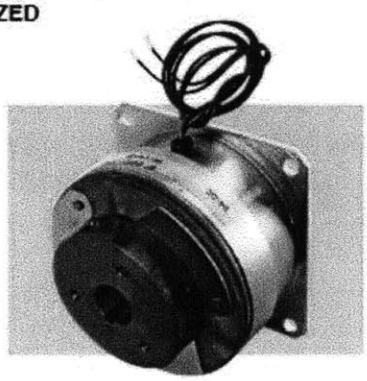

Catalog Number	Static* Torque lb. in.	Nominal Resistance ohms	Max. Watt-age	Armature Inertia lb. in. sec²	Energy Dissipation lb. ft./min.	Armature Engagement msec	Armature Disengagement msec	P Bore
S90BF9-11A04	5	128	5	3.4×10^{-5}	175	5	18	.250
S90BF9-17A04	15	108	6	8.1×10^{-5}	420	10	27	.250
S90BF9-22A06	40	75	8.5	33.1×10^{-5}	1400	12	32	.375
S90BF9-26A06 S90BF9-26A08	80	66	9.5	81.0×10^{-5}	2600	15	35	.375 .500
S90BF9-30A10 ΔS90BF9-30A12	125	43	15	179.5×10^{-5}	2900	18	45	.625 .750

Catalog Number	A Max.	B	C	D	E Max.	F	G	K** Max.	Weight lb.
S90BF9-11A04	1.25	1.498	1.31	.125	1.17	.05	.53	1.14	.2
S90BF9-17A04	1.78	2.436	2.13	.187	1.82	.06	.75	1.27	.5
S90BF9-22A06	2.26	2.873	2.50	.166	2.33	.06	.88	1.74	.9
S90BF9-26A06 S90BF9-26A08	2.63	3.499	3.13	.187	2.63	.06	1.06	1.84	1.2
S90BF9-30A10 ΔS90BF9-30A12	3.27	4.186	3.75	.187	3.25	.09	1.75	1.93	3

NOTE: Other voltages available on special order.

*Typical torque after burnishing; units shipped burnished.

**For Catalog Numbers: -11A04, initial working air gap at installation shall be .004/.009.
-17A04,-22A06, -26A06, -26A08, initial working air gap at installation shall be .006/.013.
-30A10, 30A12, initial working air gap at installation shall be .008/.018.

ΔWill be discontinued when present stock is depleted.

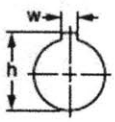

Keyway Dimensions					
Bore	.250	.375	.500	.625	.750
h	.286	.425	.564	.709	.837
w	.062	.094	.125	.188	.188

13-42 REV: 1-18-07 JC

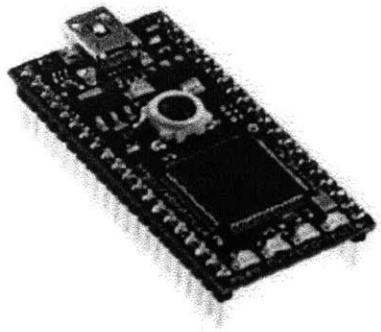

mbed NXP LPC1768 prototyping board

Rapid prototyping for the LPC1768 MCU

This board, which works with the groundbreaking mbed tool suite, lets you create a functioning prototype faster than ever. The tightly coupled combination of hardware and software makes it easy to explore designs quickly, so you can be more adventurous, more inventive, and more productive.

Features

- Convenient form-factor: 40-pin DIP, 0.1-inch pitch
- Drag-and-drop programming, with the board represented as a USB drive
- Best-in-class Cortex-M3 hardware
  - 100 MHz ARM with 64 KB of SRAM, 512 KB of Flash
  - Ethernet, USB OTG
  - SPI, I²C, UART, CAN
  - GPIO, PWM, ADC, DAC
- Easy-to-use online tools
  - Web-based C/C++ programming environment
  - Uses the ARM RealView compile engine
  - API-driven development using libraries with intuitive interfaces
  - Comprehensive help and online community

Benefits

- Get started right away, with nothing to install
- Get working fast, using high-level APIs
- Explore, test, and demonstrate ideas more effectively
- Write clean, compact code that's easy to modify
- Log in from anywhere, on Windows, Mac or Linux

The mbed NXP LPC1768 board lets you create prototypes without having to work with low-level microcontroller details, so you can experiment and iterate faster than ever.

Designers compose and compile embedded software using a browser-based IDE, then download it quickly and easily, using a simple drag-and-drop function, to the board's NXP Cortex-M3 microcontroller LPC1768.

Engineers new to embedded applications can use the board to prototype real products incorporating microcontrollers, while experienced engineers can use it to be more productive in early stages of development. The mbed tools are designed to let you try out new ideas quickly, in much the same way that an architect uses a pencil and paper to sketch out concepts before turning to an advanced CAD program to implement a design.

NXP founded by Philips

Elegant simplicity

The mbed tool has been designed for the best trade-off between versatility and immediate connectivity. The LPC1768, housed in an LQFP package, is mounted on the mbed board, which uses a 40-pin DIP with a 0.1-inch pitch. The convenient form factor works seamlessly with solderless breadboards, stripboards, and PCBs.

There is no software to install – everything, even the compiler, is online. The compiler and libraries are completely modular, so they're easy to use, yet powerful enough to take on complex, real-world applications.

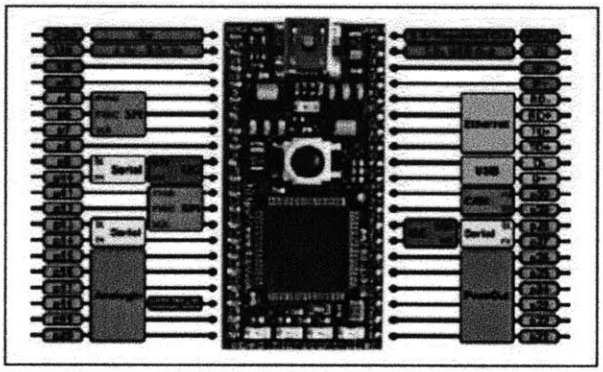

Pinout diagram of mbed NXP LPC1768 board

Hassle-free startup

Getting started is as simple as using a USB Flash drive. Simply connect the mbed NXP LPC1768 board to a Windows, Mac or Linux computer and it will appear as a USB drive. Follow the link on the board to connect to the mbed website, where you can sign up and begin designing. There are no drivers to install or setup programs to run. It's so easy, in fact, that you can have a "Hello World!" program running in as little as five minutes.

Online compiler

The mbed Compiler lets you write programs in C++ and then compile and download them to run on the mbed NXP LPC1768 microcontroller. There's no need to run an install or setup program, since the compiler runs online. Supported browsers include Internet Explorer, Firefox, Safari, or Chrome running on a Windows, Mac, or Linux PC. You can log in from anywhere and simply pick up where you left off. And, since you're working with a web-based tool, you can be confident that it's already configured and will stay up-to-date.

The compiler uses the ARM RealView compile engine, so it produces clean, efficient code that can be used free-of-charge, even in production. Existing ARM application code and middleware can be ported to the LPC1768 microcontroller, and the mbed tools can be used alongside other professional production-level tools, such as Keil MDK.

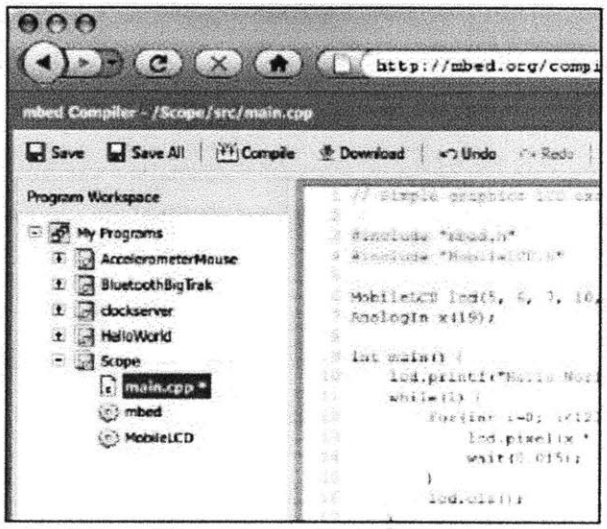

The mbed Compiler

Peripheral libraries

The mbed Library provides an API-driven approach to coding that eliminates much of the low-level work normally associated with MCU code development. You develop code using meaningful peripheral abstractions and API calls that are intuitive and already tested. That frees you up to experiment, without worrying about the implementation of the MCU core or its peripherals. You can work faster and be more creative, and can concentrate on exploring and testing the options for your design.

Rather than simply providing examples, mbed focuses on reusable library functionality, with clear interfaces and solid implementations. The core mbed Library supports the main LPC1768 peripherals, and the libraries already contributed by the mbed design community include USB, TCP/IP, and HTTP support. It's also possible to add third-party and open-source stacks.

The libraries comply with the ARM EABI and are built on the Cortex Microcontroller Software Interface Standard (CMSIS),

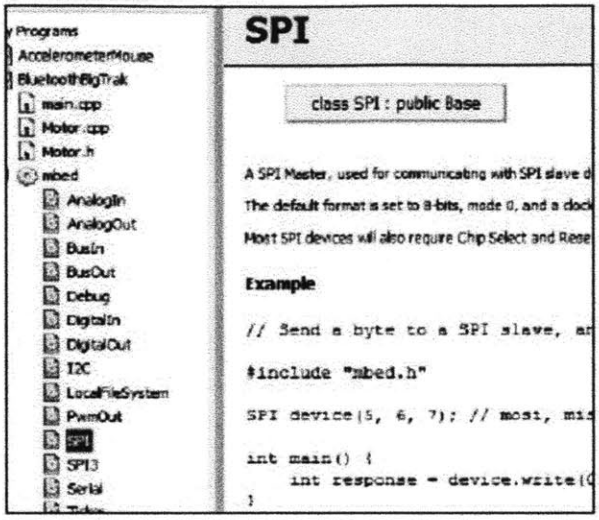

The mbed Library

making it possible to migrate to other toolchains or implement custom code for peripheral interfaces.

LPC176x microcontrollers

The NXP microcontroller family LPC176x is a series of cost-effective, low-power Cortex-M3 devices that operate at up to 100 MHz. They feature best-in-class peripheral support, including Ethernet, USB 2.0 host/OTG/device, and CAN 2.0B. There are 512 KB of Flash memory and 64 KB of SRAM. The architecture uses a multi-layer AHB bus that allows high-bandwidth peripherals such as Ethernet and USB to run simultaneously, without impacting performance. The family is pin-compatible with NXP's 100-pin LPC236x series of ARM7-based microcontrollers.

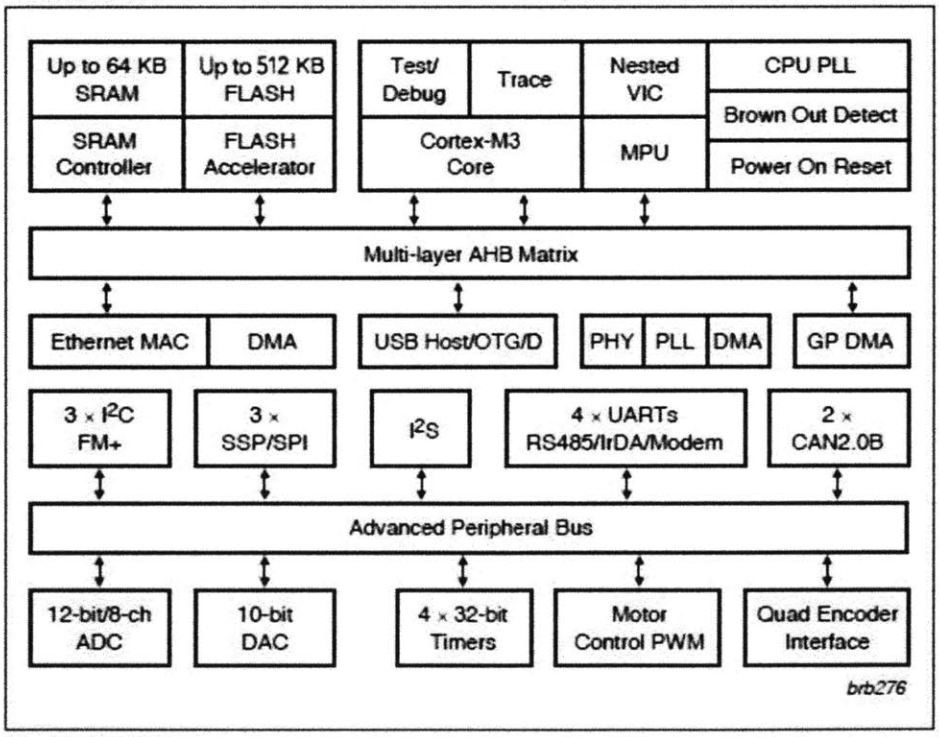

LPC1768 block diagram

LPC1768 features

ARM Cortex-M3 core	• 100 MHz operation • Nested Vectored Interrupt Controller for fast deterministic interrupts • Wakeup Interrupt Controller allows automatic wake from any priority interrupt • Memory Protection Unit • Four reduced-power modes: sleep, deep sleep, power-down and deep power-down
Memories	• 512 KB of Flash memory • 64 KB of SRAM
Serial peripherals	• 10/100 Ethernet MAC • USB 2.0 full-speed device/Host/ OTG controller with on-chip PHY • Four UARTs with fractional baud rate generation, RS-48, modem control, and IrDA • Two CAN 2.0B controllers • Three SSP/SPI controllers • Three I²C-bus interfaces with one supporting Fast Mode Plus (1-Mbit/s data rates) • I²S interface for digital audio
Analog peripherals	• 12-bit ADC with eight channels • 10-bit DAC
Other peripherals	• Ultra-low-power (< 1 uA) RTC • General-purpose DMA controller with eight channels • Up to 70 GPIO • Motor control PWM and Quadrature Encoder Interface to support three-phase motors • Four 32-bit general-purpose timers/counters
Package	• 100-pin LQFP (14 x 14 x 1.4 mm)

mbed

http://mbed.org

Date of release: September 2009

Document order number: 9397 750 16802

Printed in the Netherlands